DESIGN, FABRICATION AND TESTING OF TWO DIMENSIONAL RADIO-FREQUENCY METAMATERIALS

THESIS

Russell P. Krones, Captain, USAF

AFIT-ENG-14-M-45

DEPARTMENT OF THE AIR FORCE
AIR UNIVERSITY

AIR FORCE INSTITUTE OF TECHNOLOGY

Wright-Patterson Air Force Base, Ohio

AFIT-ENG-14-M-45

DESIGN, FABRICATION AND TESTING OF TWO DIMENSIONAL RADIO-FREQUENCY METAMATERIALS

THESIS

Presented to the Faculty

Department of Electrical Engineering

Graduate School of Engineering and Management

Air Force Institute of Technology

Air University

Air Education and Training Command

In Partial Fulfillment of the Requirements for the

Degree of Master of Science in Electrical Engineering

Russell P. Krones, BS

Captain, USAF

March 2014

AFIT-ENG-14-M-45

DESIGN, FABRICATION AND TESTING OF TWO DIMENSIONAL RADIO-FREQUENCY METAMATERIALS

Russell P. Krones, BS

Captain, USAF

Approved:

//Signed//	3 Mar 2014
Derrick Langley, Maj, USAF, PhD (Chairman)	Date
//Signed//	3 Mar 2014
Peter J. Collins, PhD (Member)	Date
//Signed//	3 Mar 2014
Ronald A. Coutu, Jr., PhD (Member)	Date

AFIT-ENG-14-M-45

Abstract

This project focused on radio frequency (RF) metamaterials (MTM) structures using two different methods: wet etching copper (Cu) on insulating glass reinforced epoxy resin (FR4) and silver nano-particle ink printed SRR meta-atoms on photo paper (Ag on paper).

Once the MTMs were fabricated, RF properties were measured using a 0-4 GHz stripline and the 2-18 GHz broad antenna near-field test and measurement range two dimensional focus beam system. Through electromagnetic (EM) material property extraction of these RF measurements, the EM properties of the MTM were also shown. Three tests were employed: scattering parameter measurements, near-field testing, and empty PPWG application testing. Results from the RF testing showed that the highest performing MTM was the Ag on paper with FR4 backing. These devices performed closest to analytic modeling and showing resonance within .4% of simulations (2.56 GHz to 2.57 GHz). This sample also displayed the best null at -21 dB, which was 3 dB lower than the Cu on FR4.

These results could be used in a number of applications, including RF absorbers or RF cloaking devices. We have successfully shown a fully capable metamaterial testing system including material property extraction.

Thank-you to God, my wife and family…all of those who believed in me most when I doubted.

Acknowledgments

I would like to express my sincere appreciation to my faculty advisor, Maj Derrick Langley, for his guidance, support and patience throughout the course of this thesis effort. The insight and experience was certainly appreciated. Major thanks to Charlie in the LORELab, I would have been lost without his help and technical expertise. Also, thanks to Dr. Collins, your insights were absolutely invaluable. Finally, thanks go to Dr. Coutu for the advice to put me on this great project with a great advisor!

Thanks to the MEMs guys for your moral support (and not killing me over the UA project, my wife also appreciated that). To my wife, sons, and family back home thanks for the prayers.

Russell P. Krones

Table of Contents

Page

List of Figures

Page

List of Tables

Page

DESIGN, FABRICATION AND TESTING OF TWO DIMENSIONAL RADIO-FREQUENCY METAMATERIALS

I. Introduction

The term metamaterials (MTMs) describes a broad area of devices with many specific definitions that share a few common elements. Ciu *et al*. describe a MTM as "a macroscopic composite of periodic or non-periodic structure, whose function is due to both the cellular architecture and the chemical composition" [1]. This definition shows the broad spectrum of topics within MTM research. To narrow this definition, Ciu *et al.* also state that the cell size needs to be less than the "sub-wavelength" if an MTM is to be regarded as an effective medium [1] or homogeneous matter. This caveat also plays an important role in the measurement of these materials. Making the assumption of a homogeneous medium leads to isotropic material equations; for these, a more simplified closed form solution exists to calculate the constituent electromagnetic (EM) properties. Therefore, this investigation focused on designing and measuring radio frequency (RF) MTM structures. Then, from the RF measurements, constituent EM material properties were derived.

This chapter is laid out in three sections. First, a background summary and problem description is given. Then the background is followed by a solution method including the limitations found and assumptions needed. The second section also details the standard of success for the solution and a summary of the implementation process. Finally, a description of the equipment and personnel needed to complete the research for this thesis are explained.

Background

Many studies pertain to MTMs even within the given definition. Some studies started as early as 1850, and began effective medium theory [2]. MTM studies evolved into more current work, including optical MTMs using individual atoms and cloaking objects by routing EM power around an object [3]. Some of the papers pivotal to MTM work are described by Shamonina and Solymar [2]. The first paper they discuss was written in 1968 by Veselago titled: "The Electrodynamics of Substances with Simultaneously Negative Values of ε and μ" [4]. In this paper, Veselago describes the effects of a medium with negative permittivity (ε) and negative permeability (μ) on electromagnetic wave propagation. In this paper Veselago includes some terms that have become synonymous with MTMs: left-handed and right-handed mediums. A left-handed medium refers to a material with a negative index of refraction, and generally negative ε and μ. A right-handed medium refers to a material with positive index of refraction, or a dielectric medium [4]. Veselago's work was dismissed as impossible, even in the conclusion of his paper, because no natural medium had been found at that time that could give a response to validate his mathematical theories.

Upon examining the other studies mentioned by Shamonina and Solymar, along with other MTM literature, two others offer useful insight to this work. Pendry *et al*. continued work on Veselago's theories in 1996 with a description of periodic wire structures as a way to achieve a negative permittivity effect in frequencies below ultraviolet wavelengths [5]. The benefits they suggested were twofold. First, the properties desired occur in lower frequencies and second, the periodic structures are lighter than the natural materials this effect occurs in. Pendry *et al*. released a

complementary paper in 1999; this paper discusses three structures that accommodate negative permeability [6]. Smith *et al*. verified Pendry's two papers in 2001 with experimental analysis [7]. These papers (Veselago's 1968, Pendry *et al*. in '96 and '99, and Smith *et al.* in 2001) started an interest in periodic structures that supports applications, including beam steering as well as the possibility of invisibility cloaking.

The Short Term Problem

The problem with these applications and structures is the lack of standard description in their experimental analysis. Most analyses contain a description of the application and do not describe the material itself. Faris suggests a solution to this problem: a standard testing device that could include scattering parameters (s-parameters) over a large frequency range and near field scanning to show the wave material interactions [8]. This solution creates a more holistic approach to describing any material as well as the design's function. S-parameters show the transmission and reflection of the material and are also used to derive the effective material properties, impedance, and index of refraction [9]. Then the near-field scans depict "wave-material interaction" [8].

These measurements can show the reaction from MTM structures in a standard way through the data gathered in testing. When this device is employed, a design used for one problem can be more readily accepted for another problem that may not be the same. However, Faris's test device lacks significant measurements for initial comparison, nor has there been any method shown for retrieving constituent EM properties using measurements from the device. Faris focused on the creation and characterization of the testing device. Other investigations in this area either used a three dimensional focus beam system or focused on modeling MTM effects. Some small scale

testing and prototype sections of MTMs have also been accomplished, like the investigations described by Langley with meta-atoms [10].

The research I propose is then the next increment in the experimental study and analysis of MTMs, with measurement and analysis of two dimensional (2-D) MTM structures. The analysis for this work also includes a method for retrieving the constituent EM material properties from a MTM. This work is bound by current theory in MTM design and lays ground work for further study into 2-D MTM structures.

Proposed Scope and Solution

Solving the problems discussed takes some assumptions, and using the desired testing device imposed some limitations. The limitations found are reviewed to show some basis for the assumptions that were made. Following the limitations, the assumptions that built the scope limiting the research and framing the solution are noted. Then the standards and criteria used to rate measurements and data are presented. Finally, the approach used to reach the solution is briefly outlined.

Limitations

Before defining the scope of this problem, it is necessary to identify the category under metamaterials that I am researching. The MTM structures created were homogeneous constructions of periodic sub-wavelength cells (meta-atoms); they were designed to present left-handed effects in the desired frequency range. This definition was used to limit the range of devices to those within the range of fabrication and testing capabilities available. Limitations noted were derived from the testing and fabrication capabilities of the Air Force Institute of Technology (AFIT) coupled with the desired outputs for analysis.

First, the demonstrated RF testing capability for metamaterials at AFIT includes a 0-4 GHz stripline, the broad antenna near-field test and measurement range (BANTAM) (a 2-18 GHz measurement range), and the GTRI focus beam system (FBS). This work was focused on 2-D MTM measurements and analysis. Therefore, only the stripline and BANTAM were utilized. The limitations from the testing equipment are mostly derived from the BANTAM, which imposed two main limitations based on the desired measurements: size and frequency.

The BANTAM is a parallel plate wave guide (PPWG) system; and therefore, the plates need to be within a certain distance of each other for the proper propagation of an EM wave. This capped the height of materials at 50.8 mm. This system also included lenses for some measurements, and in order to fit between the lenses, the material had to be 482.6 mm or less. Finally, the near-field scans made the top plate of the PPWG move. To keep from damaging the anechoic siding these scans could be no wider than 362 mm.

Frequency was limited because of the desired measurements. The BANTAM 2-D FBS excited its first higher order transverse electric and magnetic (TEM) mode at 2.95 GHz. Any measurements above this frequency could not be used for constituent material property extraction. Therefore, the frequency was limited to the 2-3 GHz range.

The desired measurements further restricted the size and compilation of the MTMs. Two lens sets were available for measurements, and in order to use less material and still get the necessary measurements, the small lens set was chosen. This reduced the possible length from 482.6 mm to 406.4 mm. Then, the calibration required the front end of the MTM to be behind the center of the lenses, so only 203.2 mm of the 406.4 mm length could be used. Finally, the moving top plate of near-field scanning measurements

caught several MTM samples, so the height had to be 49.5 mm or less so it would not be caught and broken, or moved. Therefore, the devices were limited to 49.5 mm x 203.2 mm x 362 mm in total size and had to be designed within a frequency of 2-3 GHz.

One other limitation is derived from the fabrication capabilities available. The two methods utilized for this research include copper on a woven glass board reinforced with epoxy (Cu on FR4) and silver nano-particle ink printed on Epson photo-paper (Ag on paper). These two methods have approximately the same resolution limit of approximately 50 μm [11]. This resolution is more than 10 times greater than the current resolution limits of microelectronic fabrication at AFIT which is at 0.5 μm. The issues that arise from this include rough edges and inconsistent sizes. These issues can lead to inconsistent measurements and only gets worse as the frequency of interest increases. However, due to the lower frequencies used for this research, this is not a significant problem.

The more pressing issues with the two chosen materials are over-etching with the Cu on FR4 and delamination with the Ag on paper. Over-etching leads to significant deviation in size and shape, as well as completely removing finer features. This problem leads to unpredictable behavior in any over-etched sample measurements. The complementary issue with Ag on paper is delamination. This can be caused by several factors from poor adherence to the substrate (photo-paper in this case), thickness of the printed material, and brittleness of the silver layer. The effect of these issues is discussed in more detail with the experimental results.

Assumptions

A few assumptions also applied. It was assumed that the meta-atom prototype effects would be similar to, if not the same as, the MTM with the same design. This was accomplished by making all measurements within the fundamental TEM mode. This method allowed for the application of well documented constituent EM parameter extraction methods. Another assumption was that the low density foam sample holders did not have any significant effects on the system. These holders were necessary to place samples consistently, and to construct the MTM sample. The last assumption applied was that the three-short calibration method could be appropriately applied for the PPWG system just like it was for both the stripline and the GTRI FBS [12]. This calibration method was vital to retrieve the constituent EM material properties. These assumptions establish some extra boundaries, and limit the scope of this research.

Standards

Within the scope described, the appropriateness of this research is evaluated through validation of theory. To that end, measurement of s-parameters, to extract effective relative permeability (μ_{eff}) and permittivity (ε_{eff}) was accomplished and compared to a model described in literature [8] [10] [13]. The extracted permeability and permittivity were compared to other MTM samples and a static dielectric media (acrylic). These comparisons help to describe dielectric and paramagnetic material under terms common in this area, such as right- or left-handed or combined behavior. With the limitations noted, the assumptions stated, and the standards outlined, the next section involves describing the approach used to gather the data to solve the problem.

Approach

To thoroughly investigate this problem within the scope described, some investigative questions needed to be answered. To start with: what design will be used? This question was paramount, as Pendry *et al.* show [5] [6], because different periodic structures affect permittivity and permeability. Moreover, many different meta-atom geometries are shown in literature [14]-[15]. To ensure repeatability and comparability to other measurements in literature, a simple geometry was best. Due to well documented analytical approaches, the design shown by Langley [10] was chosen. This design was successful in demonstrating active tuning capabilities in his research [10] [16]. This design was also created to affect both μ_{eff} and ε_{eff}, which should give a left-handed response in the resonant frequency.

Next: does the design resonate at the desired frequency and why? To answer this, two methods were employed: modeling and prototyping. For this application, many models have been used, so a both an analytic model and a simple simulation model were applied. When the models were within the desired range a prototype was fabricated and measured. This experimentally determined the center frequency by viewing the raw data. The prototype data gave a quick representation design, and presented some possible flaws in the model.

After the prototype was tested and evaluated the next question was: Could the 2-D structure be built given this data? When the desired resonant frequency was achieved, showing a significant resonant null, the 2-D structure was fabricated and tested based on the designs. The MTM tests included measuring s-parameters and near-field scanning. S-parameters were used to show the resonant null(s) and, when processed, the effective

parameters. The near-field scanning showed the EM wave material interactions, and when applied in different configurations some applications were apparent.

The final question was: Did the result follow established theory? When the raw data were processed and compiled, the prototype measurements were compared to the models. Then the stripline measurements were compared to the MTM s-parameter measurements. Where the results were too far from theory and modeling, the issues were discussed and theories were extrapolated based on the measurements.

Initial Look at Processes and Equipment

The approach described here was supported by many pieces of equipment for design, fabrication, testing, and finally interpretation. In the design process three computational tools were used. First, Matlab was required. Matlab was used for all aspects of this research, but for the design stage it was used to run the numeric calculations and compile the simulation results. Second, a layout editor (L-Edit) was used to draw the designs calculated and convert the designs to files for fabrication and simulation. Third, CoventorWare® was employed to simulate the device. After design the fabrication, equipment required was for creating copper on insulating glass reinforced epoxy resin (FR4) board (Cu on FR4) meta-atoms and printing silver meta-atoms on photo-paper.

For the two fabrication processes utilized only one was accomplished in-house: the Cu on FR4 board. The other samples fabricated were made from silver nanoparticle ink printed on photo-paper (Ag on photo-paper). The Cu on FR4 fabrication method started with black painted Cu on FR4 board. This board was laser etched to create the desired pattern. Then the patterned Cu on FR4 was soaked in a copper etchant leaving only the desired pattern in copper. The Ag on photo-paper MTM was printed using the

design file. However, this printing needed some conversion of the design sizing to get the desired output dimensions. This conversion was based on the ink used, what the devices were being printed on, and the desired thickness of silver (which also requires multiple prints, one on top of the other). Therefore, this method needed a specialist to create the devices; they were fabricated thanks to Capt. Jack Lombardi and the AFRL Sensors Directorate.

Next, to gather all of the necessary RF test data, two RF test set-ups were required. The first was for the one dimensional (1-D) meta-atom prototype (the 0-4GHz strip line) with an associated programmable network analyzer (PNA) to gather s-parameters. The second test set-up was for the 2-D MTM samples, which was the BANTAM 2-D FBS. The BANTAM 2-D FBS has an intended measurement range of 2-18GHz, and outputs individual s-parameters based on several measurement configurations. Finally, to interpret this data, Matlab code was used again. Here Matlab code converted the raw data into plots and calculated ε_{eff} and μ_{eff}.

Other support vital to the completion of this research included help from the Low Observable Radar and Electromagnetics Laboratory (LORELab) technician. The LORELab technician wrote the code that connected the PNA and the BANTAM 2-D FBS and facilitated the appropriate use of calibrations, connections and repair of this test set-up. Lastly, and possibly the most important, financial help from the Office of Special Research was used to purchase some materials needed to create the devices tested.

Experimentally validating theory through design and fabrication of 2-D devices is the next step in microwave metamaterial research at AFIT. This research leads to a better description of microwave MTMs, and can be a stepping stone for further research in

tunable MTM measurement and characterization. This research also validates the work accomplished by Collins and Farris through the creation of the BANTAM 2-D FBS [8] and fulfilled some of the future work suggested by Langley [10].

Thesis Layout

This thesis contains five more sections. The next chapter discusses literature and experiments relevant to the problem as well as the theory behind the measurements and EM property extraction. The third chapter describes the methodology used to gather the data. Chapter four describes the data from prototype validation to MTM application measurements and gives analysis for the measurements. Conclusions from both the experiments and analysis are provided in chapter five, as well as some recommendations for actions and future work. The final section (Appendices) describes some background work to validate the precision of the BANTAM 2-D FBS, the less used large lens measurements, and further near-field measurement.

II. Literature Review

The topic of metamaterials includes many different effects and media. A precise definition narrows the subject and describes the effect and medium of interest. The definition Ciu *et al.* give for metamaterials (as stated in Chapter 1) which is most useful for this research: "A periodic array of conducting elements [that] can behave as an effective medium for electromagnetic scattering when the wavelength is much longer than both the element dimension and the lattice spacing" [3]. Using this definition, the type of device or medium (periodic array of conducting elements) and the effect we want (electromagnetic scattering) are both described.

In metamaterial (MTM) research, the first person to suggest negative permittivity and permeability was Veselago (1968). This work inspired the theories of Pendry *et al*. on devices that achieve these effects. The periodic devices Pendry *et al.* develop in their 1996 [5] and 1999 [6] papers were experimentally verified by Smith *et al*. in 2000 [7]. These papers started a wave of research into the possibilities of the effects Veselago first described. First generation devices were similar to those described by Langley as meta-atoms or the individual cells of an MTM structure [10].

Meta-atoms are designed to resonate at the desired frequency; this achieves a relative permittivity (ε_r) and/or relative permeability (μ_r) not natural to the materials that comprise the meta-atom. The effective parameters comprise four different effects based on their signs (positive or negative) as shown in Figure 1. This figure shows the effects Veselago described as left and right handed (both ε_r and μ_r positive or both negative), and the plasma or ferromagnetic effects that are described by Pendry *et al*. [5] [6]. Throughout this chapter we will discuss theory that supports radio frequency (RF) MTM

research, some of the history behind this research, and some places where this research is applicable.

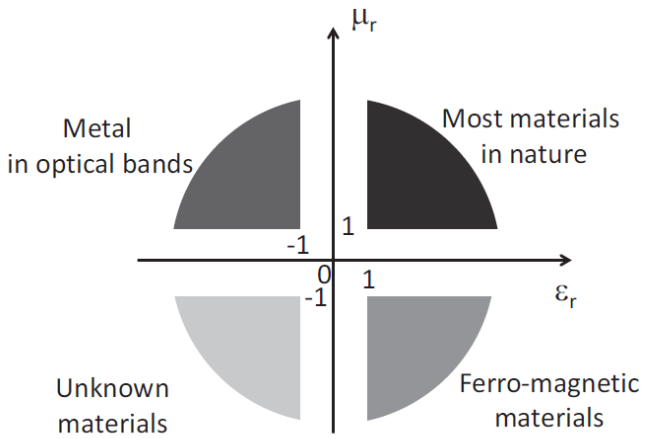

Figure 1 Categories in the relative ε-μ domain [14]

Abbreviated Metamaterial History

In electromagnetic (EM) theory there are two basic reactions when an EM wave interacts with a dispersive medium: reflection or refraction. When the permittivity and permeability of a medium are positive, a wave reflects off, but when either permittivity or permeability is negative, the incident wave is refracted at an angle, described by Snell's Law, within the medium:

$$\frac{\sin\varphi}{\sin\psi} = \frac{n_2}{n_1} = \sqrt{\frac{\varepsilon_2\mu_2}{\varepsilon_1\mu_1}}\,. \tag{1}$$

Here φ is the incident angle of the wave, ψ is the reflected/refracted angle, and n_1 and n_2 are refractive indexes of the first and second media. Veselago noted that there was no description at that time of what would happen if that medium had both negative permittivity and permeability. To describe what effect(s) might be observed he started with the dispersion equation.

The dispersion equation takes a simpler form in isotropic substances:

$$k^2 = \frac{\omega^2}{c^2} n^2 . \tag{2}$$

Here k is the wave vector, ω is the radial frequency of the wave vector, c is the speed of light, and n is the index of refraction. The index of refraction is further described by:

$$n^2 = \varepsilon\mu . \tag{3}$$

Where ε and μ are the permittivity and permeability of the medium with which the wave is interacting. Veselago shows that if these equations are used with mathematical interpretations, instead of physical descriptions, we can write Snell's Law as:

$$\frac{\sin\varphi}{\sin\psi} = \frac{n_2}{n_1} - \frac{p_2}{p_1}\left|\sqrt{\frac{\varepsilon_2\mu_2}{\varepsilon_1\mu_1}}\right| . \tag{4}$$

This equation uses p_1 and p_2 as the "rightnesses of the first and second media" [4]. These equations show a response, like ray 3 shown in Figure 2, which creates the "reflection" through a left-handed material. Although Veselago describes this derivation as mathematically abstract, he notes where these effects might be found in nature. At the time of Veselago's writing there were no experimental data to support his suppositions.

Pendry *et al*. in 1996 describe a periodic structure of thin wires that fit the previous definition for an MTM [5]. This arrangement is intended to achieve an electric plasma effect (Quadrant 2 of Figure 1), but in the gigahertz (GHz) range of the RF spectrum instead of the ultra-violet region where it is observed naturally in metals. The electric plasma effect is achieved through negative ε_{eff} from the resonance of the periodic structure Pendry *et al*. describe [5]. At the resonant frequency, ε_{eff} switches signs and becomes negative before returning to the original permittivity value. Pendry *et al*. follow

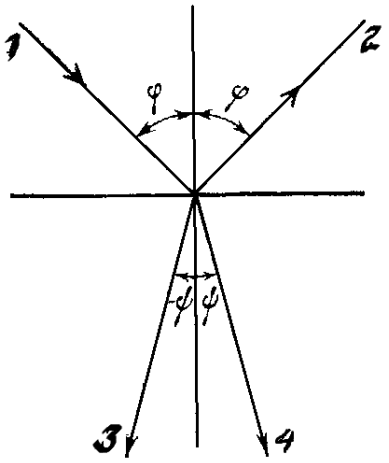

Figure 2 As shown in Veselago's Paper: Passage of a ray through the boundary between media. 1 – Incident ray; 2 – reflected ray; 3 – reflected ray if the medium is left-handed; 4 – reflected ray if the medium is right-handed [4]

this theory in 1999 with a similar discussion of periodic cylinders which present negative μ_{eff} [6]. These structures respond similarly to the thin wires, with a change in permeability instead of permittivity at the resonant frequency. The thin wire and cylinder structures were experimentally verified by Smith *et al*. They used a combination of thin wires (a negative ε_{eff} structure) and split-ring resonators (a negative μ_{eff} structure). With experimental verification of these structures, many applications have been presented from flat lenses to cloaking devices or perfect absorbers [17] [18] [19].

Theory

The research accomplished at AFIT describes the effects of 1-D MTM structures and the possibility of tuning MTMs through different MEMs structures [10] [13]. Researchers have also simulated the effects of 2-D MTM structures with various software packages and built devices to measure the effect MTMs have on EM waves [8] [9] [20]. None of this research provides comparison in experimental data on 2-D MTM devices,

but (as Smith describes) the theory involved with 1-D MTM is similar to that of 2-D MTMs [3].

Design Theory

Langley describes a simple method for designing meta-atoms using the self-inductance of the conductive traces and parasitic capacitance across the gaps of a split-ring resonator (SSR) structure combined with long thin wires. After discussing how to split the meta-atom of the MTM device into four sections, he describes how the device can be modeled as a lumped element circuit. Using this model we can calculate the resonant frequency:

$$\omega_0 \approx \frac{1}{\sqrt{\mathrm{LC}}}. \tag{5}$$

Where L is the lumped inductance, C is the lumped capacitance, and ω_0 is the resonant frequency [10]. However, Langley describes only 1-D arrays which are modeled for their tuning capability, and their resonance is verified using a stripline. This configuration is the best tool for initial analysis of the MTM design, since the scattering parameters (s-parameters) can easily be used to describe the effective parameters we are looking for ($\varepsilon_{\mathrm{eff}}$ and μ_{eff}).

Measurement Theory

The stripline is a good tool for first order measurements in 2-D MTM research since the same theory applies in 2-D analysis as in the 1-D case. For this research, this means we can estimate the resonance and 2-D response with a prototype and incur little measurement error. We can also use the same theory for retrieving effective parameters in the 1-D case to estimate the full response for design verification purposes. The 2-D

design, however, cannot be evaluated using a basic stripline. Therefore, AFIT's Broadband Antenna Near-Field Test and Measurement Range 2-D Focused Beam System (BANTAM 2-D FBS) was used. The BANTAM includes two monopole antennas that are focused with custom crafted lenses in a parallel plate waveguide system. The parallel waveguide system is encapsulated in an anechoic chamber to mitigate "the potential for external noise and clutter interference" [8]. Faris describes the design and function of the system, but for this research the primary use will be far-field s-parameter measurements, which are used to retrieve the effective permittivity and permeability.

Analysis Theory

One of the unique aspects of the work was to use the measured s-parameters to show the constituent EM material properties of the MTM. Smith *et al*. [21], Chen *et al*. [9], and Hanson *et al*. [22] describe similar methods for retrieving the effective parameters. Each of these methods derives the impedance and/or index of refraction which is used to back out ε_r and μ_r. Langley describes the s-parameters in terms of "the incident, reflected, and transmitted electric fields," and shows how these relate to impedance (z):

$$z=\pm\sqrt{\frac{(1+S_{11})^2-S_{21}^{\ 2}}{(1-S_{11})^2-S_{21}^{\ 2}}}\,. \tag{6}$$

Equation (6) shows impedance calculated using the reflected power as seen by port 1 of the measuring device (S_{11}) and the transmitted power from port 1, as seen by port 2 (S_{21}). From this point we can solve for the real and imaginary refractive index values, from which some "requirements can be imposed" [10]. These requirements are based on properties of the material being measured (whether the material is passive or contains

active components). For our purpose the material will be passive, so the real part of the impedance must be greater than or equal to zero (positive). This limit means that we assumed the medium was resistive in nature and the signal was not amplified (as an active medium might accomplish). Equation (7) and (8) relate the index of refraction (n) and impedance to both permittivity (ε) and permeability (μ). Permittivity is then:

$$\varepsilon = \frac{n}{z} \tag{7}$$

and permeability is:

$$\mu = nz\,. \tag{8}$$

In these equations ε, μ and z are all "frequency dependent complex functions that [need] to satisfy certain requirements based on causality" [10]. Using these equations and the requirements imposed, we can utilize a MATLAB script to calculate the effective parameters based on measured s-parameter data.

Measurement Applications

Literature abounds with applications for RF MTMs, ranging from lenses to absorbers, as well as antennas or antenna enabling devices. These applications all benefit from the changing relative EM material properties that are unique to metamaterials. Metamaterials changed the material search into an exacting choice since the EM properties can be explicitly designed [19]. With MTMs nearly any relative EM material properties can be achieved. Here we discuss three main applications for metamaterials which could find using from the BANTAM 2-D FBS. These applications are absorbers, antennas, and lenses. Some other applications that would benefit from this unique measurement system will also be discussed.

Metamaterial Absorber

As we will show later, the versatility of the BANTAM 2-D FBS lends itself to testing many different applications, as well as verifying application-based claims. One application which is discussed further in Chapter 4 is the MTM absorber. Watts, Liu and Padilla describe two main kinds of absorbers: the resonant absorber and the broadband absorber [19].

The resonant absorber utilizes a resistive material that is one quarter wave length (of the desired frequency) thick with a metal plate backing. This type of absorber would need to include multiple layers to affect multiple frequencies of interest. The broadband absorber, on the other hand, is the kind of absorber used in anechoic chambers. This type would consist of a lossy material which absorbs the signal over the length of the absorber. Metamaterial absorbers are essentially resonant absorbers; however, they are not restricted by the quarter wavelength layer, and can be significantly thinner. Moreover, absorbers were traditionally confined to frequencies below 30 GHz [19]. Metamaterials have been shown to be effective absorbers through THz frequencies [23].

Metamaterial Antennas

Another application that could be used with the BANTAM 2-D FBS is the metamaterial antenna. Several antenna designs have been shown [14] [24]-[29]. These designs include several seemingly unrelated uses of metamaterial designs that are implemented for some specific applications. However, Dong and Itoh summarize these designs into two categories: leaky wave antennas (LWAs) and resonator type small antennas [30].

The LWAs provide high directivity without requiring a complex feeding network. Metamaterial LWAs utilize the composite right-handed/left-handed transmission line metamaterial design to enable a backfire-to-endfire scan (180° scan pattern for θ=-90º to θ=90º). The limitation of this scanning field is the major drawback of non-metamaterial devices [31].

Dong and Itoh discuss four types of resonator type small antennas: dispersion engineered resonant antennas, miniaturized antennas with MTM loading, metaresonator antennas, and antennas loaded with metasurfaces. These antennas are either MTM based or utilize MTMs to increase performance. The benefits of these antennas are: reduced size, lower cost, broad bandwidth, and good efficiency [30]. Metamaterial based resonator antennas have also been used to garner better quality factor and radiation efficiency.

Dispersion engineered antennas use a composite left-hand/right-hand MTM to utilize the complementary effects to create unique affects, such as highly reduced return loss, high directivity, and polarization at the device's resonance [31]. Miniaturized antennas with MTM loading utilize the properties of MTMs to reduce the size of the antenna size and keep consistent performance. This differs from metaresonator antennas which, more like the dispersion engineered antennas, directly use MTM designs for the antenna. The benefits of this design method are derived from reduced size and increased quality factor. Finally, the antennas loaded with metasurfaces are similar to the MTM loading; in the fact that the metasurface enhances the antenna performance instead of performing the antenna function. This type of antenna has shown increased directionality and efficiency.

Metamaterial Lenses

Since the BANTAM 2-D FBS utilizes two different sets of focusing lenses, this measuring system is uniquely qualified to characterize MTM lenses. The BANTAM can be used to measure the material properties of the lens. The refraction and reflection can also be shown using near-field scanning. Metamaterial lenses were first introduced by Veselago with the supposition of a material that had simultaneously negative permittivity and permeability [4]. However, after Pendry *et al*. described devices that could attain these properties [5] [6] and Smith *et al*. showing that their implementation was possible [7], Pendry discussed the possibility of "super-lenses".

Super-lenses are lenses created with a negative index of refraction [32]. Pendry shows that this type of lens can focus even with a flat slab based on the refractive index and thickness of the material [17]. This type of lens focuses inside of the material, and again when the wave leaves the lens. These lenses have been shown in applications ranging from focusing [33] to columniation and imaging [34].

These applications utilize metamaterials to enable other technologies or increase performance of a technology. They also decrease costs by utilizing more common materials to create exotic properties. However, even this technology can be optimized. One way to decrease the cost of metamaterials and add even more unique properties is by utilizing conductive material printing techniques.

Printed Metamaterials

Many RF devices depend on traditional printed circuit board (PCB) designs [11]. For example, the first devices fabricated for this research were built from PCB. There are

benefits to this type of fabrication, which include ease of availability and abundance of fabrication methods. However, PCB boards have some drawbacks.

PCB is commonly fabricated with FR4 which is a rigid dielectric. This material is can take an extremely long time to decompose, and many of the fabrication methods include either hazardous chemicals or dangerous waste products [11]. These materials are a threat to the environment and can add costs for hazardous waste removal. One method being explored to replace this technology is printing conductive materials.

Le *et al*. describe the advantages of printing conductive materials as "low cost, scalability, [and] high repeatability…" [11]. This technique is also flexible in the type substrate (e.g. paper, plastic, quartz), and the types of materials available for printing (e.g. silver, graphene, carbon nano-tubes). Moreover, the printing process is easily within the tolerance of wet-etching PCB board fabrication (50 μm). This is not just a theoretical technology; many applications have been demonstrated from MTM absorbers [23] [35] to MTM antennas [36], and MTM based RFID tags [27] to name only a few.

Summary

Starting with a refined definition for metamaterials, the history and theory behind periodic conducting arrays was discussed, as well as describing how MTM arrays can behave like an effective medium. Different designs have been shown to affect each constituent EM material parameter, and combinations of these designs create different effects. First order design theory was described using the method shown by Langley, and some of the theory on the transition of measured data to effective parameters was also presented. This research was accomplished to demonstrate effects of metamaterials in 2-D, and to experimentally define a 2-D metamaterial structure. As discussed in Chapter 1,

this research builds on previous research and adds experimental analysis and material characterization with two dimensional (2-D) MTMs.

III. Methodology

In this chapter the methodology used in the design, fabrication, and testing of two dimensional (2-D) metamaterials (MTMs) is discussed. This methodology follows the work completed by Faris [8], Langley [10], and Gunn [12]. Within this research, a material property extraction Gunn discusses was used (without his restrictions). The testing apparatus and basic measurements created by Faris are used to measure the design, and the design methods Langley discusses are utilized to create a MTM sample. The first section details the design choices, limitations, and the two models used to derive the possible MTM structures. In the second section, the two fabrication methods used are discussed as well as the limitations each method presents. Finally, the third section describes the testing accomplished, including the need for each test in the process. The final section also discusses how the equipment outlined in Chapter 1 was used. This discussion leads into the results (presented in Chapter 4) and a discussion of the data which were collected throughout this research process.

Meta-Atom Design

Many meta-atom designs have proven successful in creating artificial dielectric and paramagnetic materials [1], [3]. These designs come in a wide variety of geometries and materials [1], [3]; however, Pendry *et al*. discuss a basic design for a paramagnetic material. The design is the split-ring resonator (SRR) like that seen in Figure 3a [6], and for the basic dielectric the thin wire structure (also described by Pendry *et al.*) shown in Figure 3b [5]. Designed and built properly together these structures have been shown to create the double negative material theorized by Veselago [4] and demonstrated by Smith *et al*. [7]. To demonstrate the ability to design, fabricate, and test MTMs, this method

incorporated both a paramagnetic and a dielectric aspect. Therefore, a design that has modeling, simulating and testing data for a smaller scale was chosen. This data was used for comparison with design choices.

a) b)

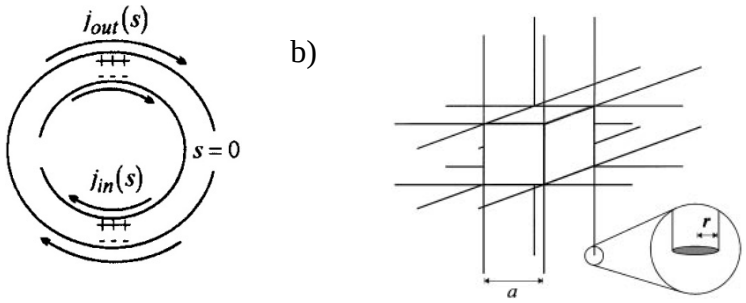

Figure 3 a) Basic split-ring resonator Pendry et al. discuss as an artificial paramagnetic material [6]. b) Depiction of long thin wire array Pendry et al. discuss to create an artificial dielectric material [5].

Langley [10] and others [3] [7] [8] describe several devices which start with a 6.35 mm thick PCB prototype. The choice to follow the design by Langley was due to the analytical and simulation methods he used to convert the meta-atom into circuit model elements. One advantage of this design methodology was the ability to compare calculated and simulated circuit elements. This assisted the comparison between the two models and previous results shown with this design. Another advantage of this methodology is the readily available data for comparison of results to ensure the prototype is performing properly. This design has also been shown effective as a base for a tunable MTM [16]. Figure 4 depicts a sample of the rectangular SRRs designed.

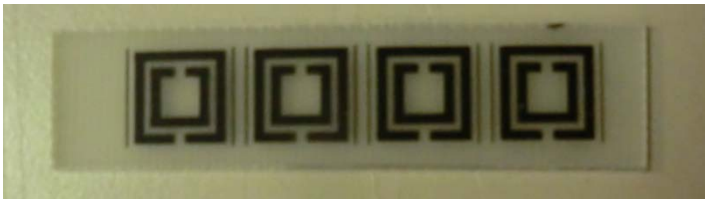

Figure 4 2.5GHz Copper on FR4 meta-atom sample

Limitations

To develop this concept into a full design, some limitations were required due to the available testing set-ups. The issues with the BANTAM 2-D FBS as discussed in Chapter 1 were the hardest to overcome. Throughout the rest of this chapter this testing device will be referred to as the BANTAM. The two largest constraints were derived from the limitations in the BANTAM's chamber. Due to the size of the antenna and lens, the chamber exhibits higher order transverse electric and magnetic (TEM) modes in the recommended frequency range. This size as discussed earlier also limits the size of the samples that can be measured when making measurements for material property extraction.

Since the process for extracting electromagnetic material properties, the measurement device must be operating in the fundamental TEM mode. Moreover, s-parameter measurements showed that any s-parameter data gathered beyond the fundamental TEM mode became unreliable, changing significantly with each measurement, and deviating from all theoretical models. According to Faris, the first higher order mode in the BANTAM was theoretically excited at 2.97 GHz [8]. Therefore, it was decided to constrain the frequencies of interest to 2-3 GHz. Second, due to the frequency range the BANTAM was designed for, the height of the material to be measured had to be slightly less than two inches (50 mm).

The stripline was designed to have a fundamental mode at frequencies up to 4 GHz. This worked well with the constriction of 3 GHz from the BANTAM. Device space for the stripline was constrained to approximately 19 mm both above and below the center conductor, which worked well with the devices designed to the BANTAM

restrictions. One final limitation evident in material property extraction came from a programmable network analyzer (PNA). The PNA used with the stripline included a factory gating package; however the PNA associated with the BANTAM did not, so post-process gating was necessary due to the difficulty in distinguishing the measured device data from the connections and cable reflections. The ability to distinguish data is readily apparent with any time domain gating; even more so with the package included with the PNA as seen in both Figure 5 and Figure 6.

a)

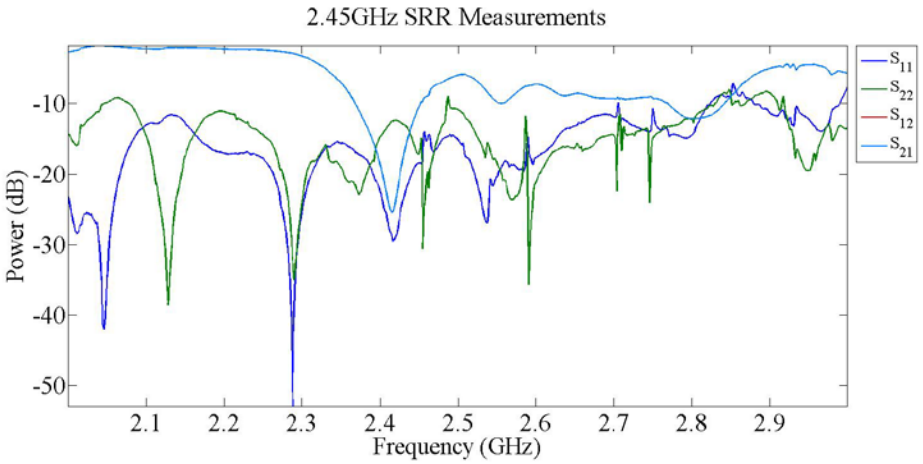

b)

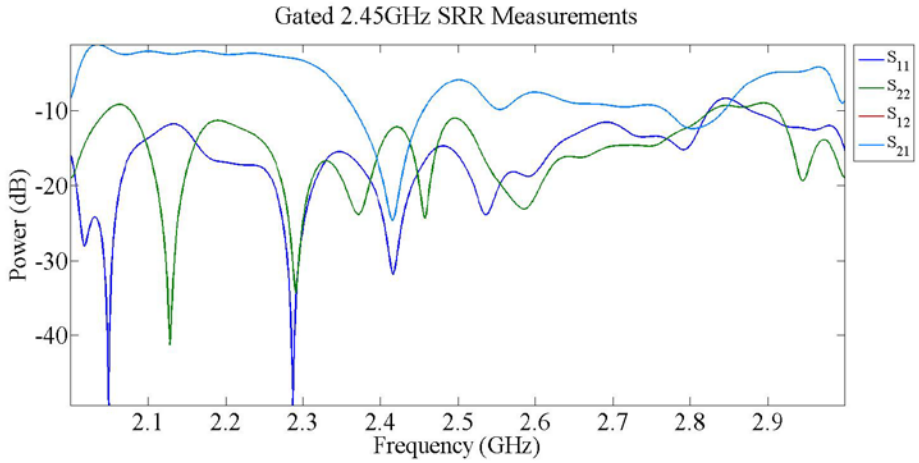

Figure 5 a) PCB fabricated sample measured without time domain gating. b) A time domain gated sample using a post-processing gating technique gating at +/-14 ns.

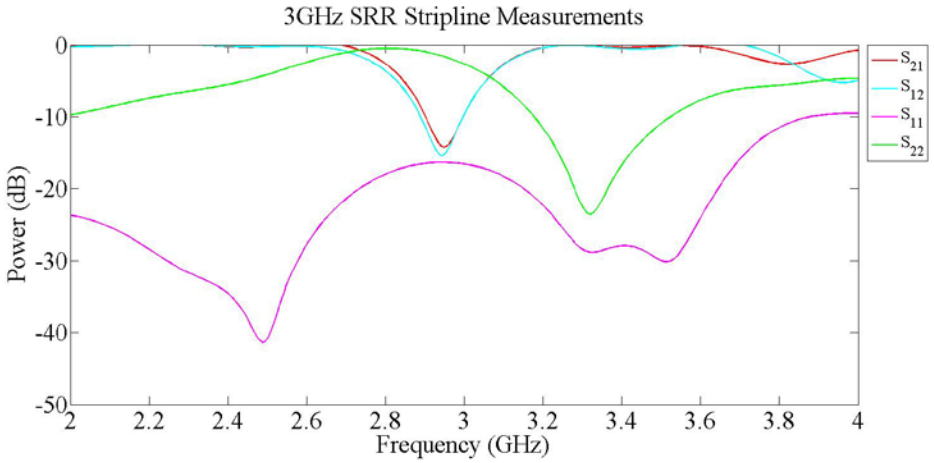

Figure 6 Cu on FR4 stripline measurement with +/-2.5 ns time gating applied by PNA

Modeling

There are several ways to design metamaterials, from the original theoretical designs by Pendry *et al*. using a completely analytical process [5] [6] to lumped element models shown by others [1] [3] [10] [37]. Each design model has advantages and drawbacks, but for this design the resonant frequency is the most desired effect. Therefore, a lumped element model was used due to the simple correlation between the lumped elements and the resonant frequency. As discussed in chapter two, this method decomposes the meta-atom in the MTM into several passive circuit elements and translates the pieces into equivalent circuit notation.

Analytic Model

Langley discussed an analytic model to convert a single SRR into circuit components [10] as shown in Figure 7. Here we illustrate the circuit elements for each method discussed in the following segments for easier understanding. The SRR is

divided into four sections, as shown in Figure 8, and for each section a capacitance and inductance is calculated.

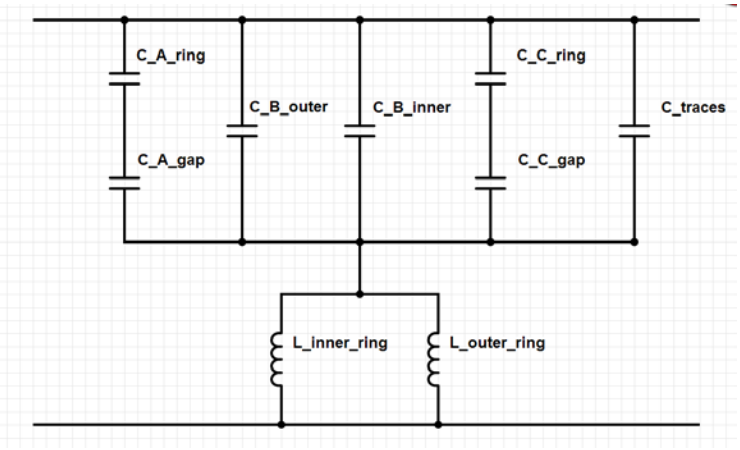

Figure 7 Shown are the seven capacitive elements and two inductive elements for the equivalent circuit model based on the four section SRR described by Langley.

The capacitance is found using a parallel plate capacitance equation. The equation we used is:

$$C = \frac{\varepsilon_0 \varepsilon_r w l}{g}. \tag{9}$$

Where C is the capacitance, ε_0 is the permittivity of free space, ε_r is the relative permittivity of the gap material (ε_r=1 for air). The gap or length between the two wire traces is g, w is the width of the wire traces, and l is the effective length. There are seven capacitance calculations, two for each section and one for the wire traces outside of the SRR. Sections A and C have two separate capacitances which are in series. These values use the series capacitance equation:

$$C = \left(\frac{1}{C_1} + \frac{1}{C_2} \right)^{-1}. \tag{10}$$

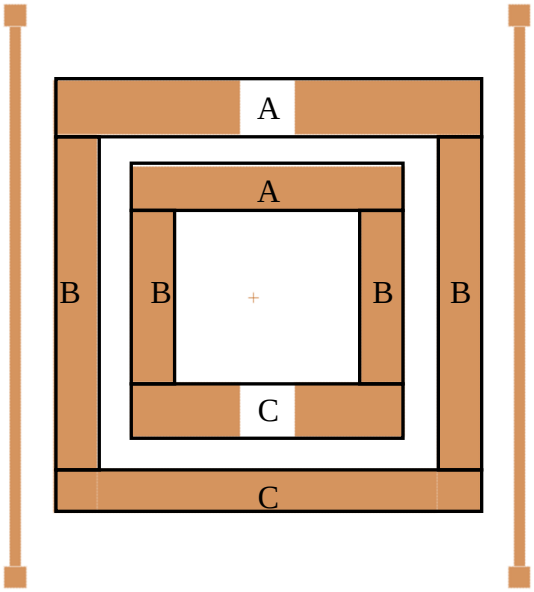

Figure 8 Four part separation suggested by Langley to derive equivalent circuit elements

Where C_1 is the capacitance due to the gap in the ring and C_2 is the capacitance between the two rings. C_1 used the length from the outside edge of the ring to the gap as the effective length. The second capacitance value (C_2) used the length from outside edge to opposite edge. As seen in Figure 8, section A used the inner ring length and section C used the outer edge length. Section B has the same width on the inner and outer rings, and the two equations use the distance between section A and B on the inner and outer rings for each of its two length variables. Finally, the traces are considered by themselves with their width, length, and the gap between section B and the traces. The series capacitances from sections A and C are in parallel with the capacitances from the section B sides and the traces on the outside. Parallel capacitance values are added together, which results in a total capacitance value for the meta-atom. Then the values are used together in the resonant frequency equations discussed in Chapter 2.

The second part of the resonant frequency equation is the inductance value. The inductance calculations, described by Ruehli [38], assume that the traces can be modeled as a long thin wire. Using equation (11) we can calculate the inductance (L) based on the dimensions.

$$\frac{L_{P_u}}{l} = \frac{\mu}{6\pi}\left\{3\ln\left[u+\left(u^2+1\right)^{1/2}\right]+u^2+u^{-1}+3u\ln\left[u^{-1}+\left(u^{-2}+1\right)^{1/2}\right]-\left[u^{4/3}+\left(u^{-1}\right)^{2/3}\right]^{3/2}\right\} \quad (11)$$

In this equation l is the length of the wire trace (the perimeter of the ring), u is the ratio of length to width, and μ is the permeability of the wire trace, which is approximately the permittivity of free space μ_0. For these calculations the outer circumference of each ring is used. The ratio u is the length of the ring in question to the thinnest width in the trace. These inductance values are treated as parallel, and just like the capacitors in series the values are calculated using:

$$L = \left(\frac{1}{L_{IR}} + \frac{1}{L_{OR}}\right)^{-1} \quad (12)$$

Here L is the total inductance of the SRR, L_{IR} is the inductance from the inner ring, and L_{OR} is the inductance from the outer ring. The wire traces are so thin relative to the SRR that their value is negligible relative to the ring traces.

CoventorWare® Simulation Based Model

To compare the circuit element values derived using the methods described previously, a finite element modeling tool, CoventorWare® was used to estimate the lumped element capacitance and inductance values for the inner ring, outer ring, and each trace. CoventorWare® is usually used for design and simulation of micro-electromechanical systems; however, this finite element modeling software is very

customizable and allows the user to implement individual processes and import designs from other programs. Any software with a significant amount of customization capability is limited by the amount of information supplied from the user. Therefore, two assumptions were made to make these simulations closer to reality. The first is that the 2-D MTM would be similar to the microelectronic fabrication processed devices described by Coutu *et al.* [16]. The second assumption was that the dimensions designed were the same as the built device. To model using this tool, the program needs four different parts: the process used to build the sample, the layout of the sample, the size and shape of the blocks to decompose the sample into for analysis (meshing), and some defined points to start and stop analysis (e.g. top and bottom, V_{in} and V_{out}).

The process upon which the simulations based its calculations was a simplified version of the process described by Coutu *et al*. [16]. The simplification was made because none of the moveable parts were associated with the meta-atoms created for this research. The process entered into CoventorWare® is only three steps: 1) start with a quartz substrate, 2) evaporate 5μm of gold on it, and then 3) etch the gold into the shape shown in Figure 9. This simplification was reasonable since the conductivity of gold, copper and silver is very close (6.30×10^7 S/m for silver, at the highest to gold at 4.10×10^7 S/m), and the final tested samples only contained a single layer of patterned metal on a substrate.

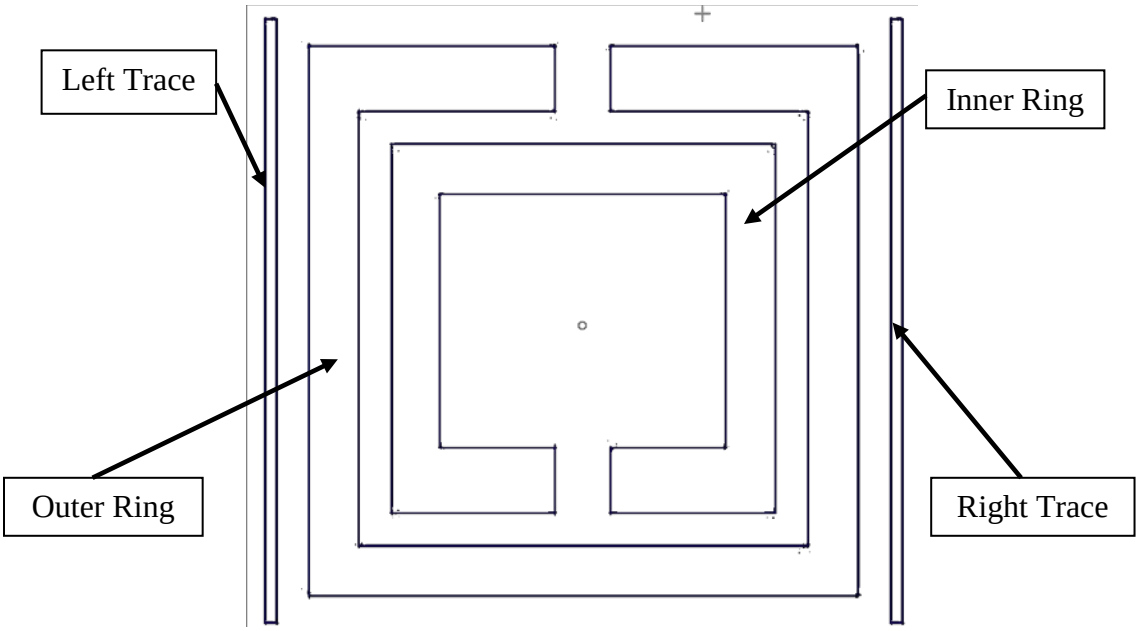

Figure 9 CoventorWare® layout

Layouts were created in L-Edit ®, a drawing tool usually used for MEMS or very large system integration circuit layouts. Figure 9 shows the imported sample drawn based on the analytical calculations described previously. These layouts were then imported into CoventorWare®, and Figure 10 is the resulting layout that the process was applied to. Once the process was applied to a layout, the mesh was applied. Before the first layout was accomplished, a quick meshing analysis was accomplished to determine how small the mesh blocks should be to have a balance between quick analysis and precise results. A simple capacitance simulation was accomplished for block sizes of: 1 mm x 1 mm x 5 µm, 500 µm x 500 µm x 2.5 µm, 250 µm x 250 µm x 2 µm. Changes between the first and second block sizes were small. Differences between the second and third block sizes were undetectable, and the simulations were quick for all sizes. We settled on a block size of 500 µm x 500 µm x 5 µm as small enough to be effective and provide quick simulations. Figure 10 shows not only the mesh blocks, but also some of

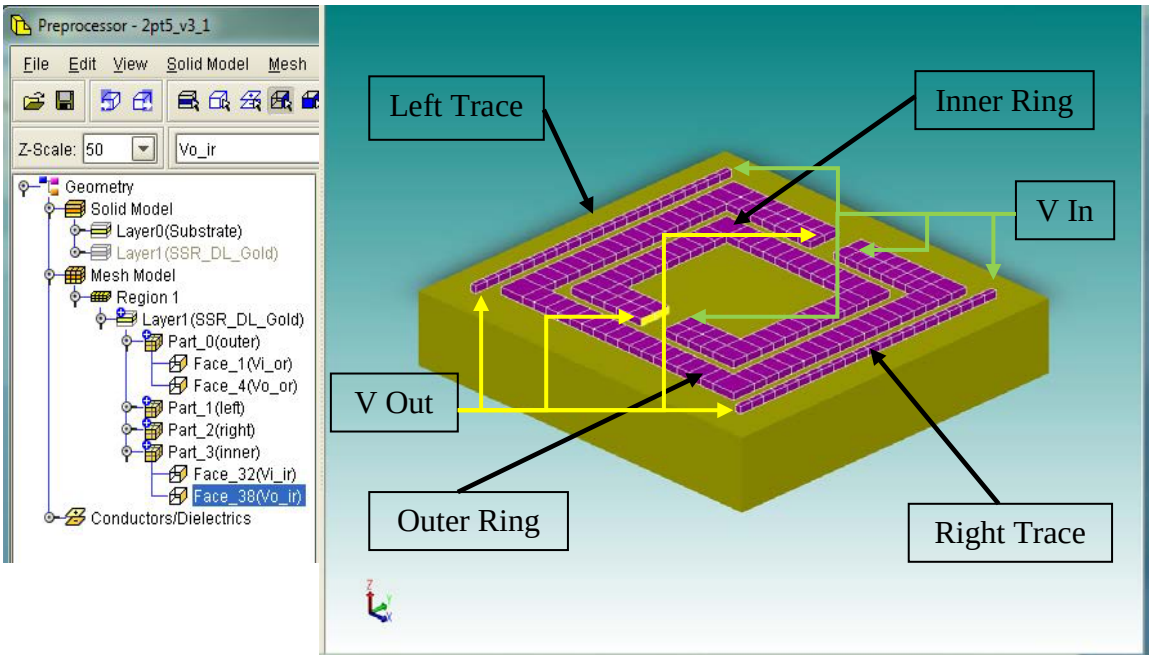

Figure 10 Sections of mesh analysis window from CoventorWare® showing the component tree and the mesh model.

the labeling. Labels were important to have on opposing sides to show a voltage in and out, thus creating the start and stop points of the analysis program. Each trace and ring was analyzed separately. Therefore, in each ring the sides of the gap were labeled for V_{in} and V_{out} as seen in Figure 10; and the traces were labeled similarly at each end.

Simulations were run for the capacitance and inductance of the device. The simulations included the start and stop points as well as the frequency range of interest. Each trace and ring was simulated separately for a frequency range of 10 MHz to 4 GHz. Since these simulations dealt with the device as two rings and two traces instead of the ABC sections in the previous analysis, a different circuit model was described as seen in Figure 11.

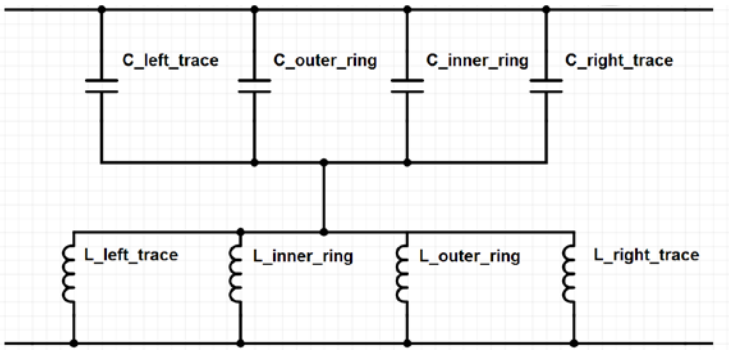

Figure 11 Circuit model based on simulated lump elements

Modeling Results

A complete model was realized with the individual parameters combined to give each a total inductance and capacitance. These numbers were used in the resonant frequency equation:

$$f_0 = \frac{1}{2\pi\sqrt{LC}}. \tag{13}$$

Here f_0 is the resonant frequency, L is the total device inductance, and C is the total device capacitance.

Keeping in mind the limitations discussed, and in order to garner the most data from the measurements range, three layouts were designed using these models. The concept we tried to attain was a near 2 GHz design, a 2.5 GHz design, and a design near 3 GHz. With the designs already described by Langley, the sizes varied from 8 mm square outer size with 2 mm gaps in the rings to a 10 mm square with 1 mm gaps. Utilizing the analytical method we previously discussed, Table 1 shows the dimensions of the three designs based on those calculations.

Table 1 Comprehensive dimensions list used for the three designs that were calculated. All dimensions given here are in millimeters.

Frequency	2GHz	2.5GHz	3GHz
IR HxL	6.7x7.0	5.7x6.0	6.2x6.5
IR W	0.9	0.9	0.9
IR Gap	1.0	0.6	1.0
Rings Gap	0.6	0.6	0.6
OR HxL	10.0x10.0	9.0x9.0	9.5x9.5
OR W	0.9	0.9	0.9
OR Gap	1.0	0.6	1.0
Trace H	11.0	10.0	11.0
Trace W	0.2	0.2	0.2
Trace Ring Gap	0.6	0.6	0.6

The results were interesting given that they were proven effective for other structures [10]. The 2 GHz dimensions gave a calculated resonance of 2.06 GHz, but the drawn design gave a simulated resonance of 2.44 GHz. This gap was similar for both the 2.5 GHz design at 2.25 GHz analytic model and 2.57 GHz simulated and the 3 GHz design at 2.31 GHz calculated and 2.82 GHz simulated.

Metamaterial Fabrication

We fabricated two types of MTM devices: a single sided PCB, which is copper on FR4, and the 2-D MTM made from silver nano-particle ink printed on photo paper. Both processes were quick and relatively inexpensive, which allows for rapid production, but each process has some drawbacks from the fabrication process.

PCB Fabrication

There were two ways to fabricate the PCB MTM samples: laser sintering or laser patterning and chemical etching. Each process has its advantages and drawbacks; however, the second process (patterning and etching) was chosen because of the well

established procedures. Benefits of this method include simplicity, a quick processing time, and no possibility of burning the FR4 board, as opposed to the laser ablation method which carries the risk of ablating past the copper and into the substrate. However, the risks from this process results from the chemical etching. Two common problems arise in the etching process: over etching or under patterning. The first risk occurs when poor etching procedures are used. Over etching causes the widths of most traces to be thinner than expected, and for thinner traces, complete delamination. Under patterning with the laser could cause sections not to pattern properly and lead to copper spurs, or over etching to remove the spurs. The guidelines for fabrication using this method were clear enough to lead to well fabricated samples if they were followed properly.

Printed Metamaterial Fabrication

Silver nano-particle ink printed on photo paper MTM devices were created for this project courtesy of Capt Lombardi and the AFRL Sensors Directorate. These devices provide an application-based dimension to the measurements in comparison to the more commonly used PCB fabricated samples and a composition material comparison. This process is like printing a picture from any inkjet printer; the difference in this instance is the special ink.

The samples created for this research utilized Epson photo paper for good ink adhesion without the absorption of the ink to the paper. A side benefit from the photo paper was that the samples were stiffer than those printed on regular printer paper. The process prints out the image a single layer at a time. Multiple layers are printed to fill defects (holes and cracks), increase conductivity, and ensure continuity. However, one issue that arose when printing was that the printed devices were different in size than

designed. This was due to the way the ink droplets formed on different materials. Therefore, a conversion factor had to be accounted for. This factor was calculated empirically by printing individual drops of ink and measuring their size (~60 μm). The design is converted to a picture file (.bmp) to get the pixel count. Then the pixel spacing was decided then to be 30 μm to allow for a 50% overlap of drops. This ensured good coverage and continuity across the printed sections. Some of the samples were measured and found to be within +/-40 μm of the design as drawn. Each device section also contained a testing bar (1 mm x 5 mm) for measuring DC resistivity, which was measured with a 4 point probe, and found to be ~0.05 ohm/sq. This measurement coupled with a thickness of ~1.25 μm gives a resistivity of ~ 8.236x10^-8 ohm-m, which is on the same order of magnitude as bulk silver.

Metamaterial Testing

Testing metamaterials (MTMs) can depend on the design, application, or equipment available. For the purpose of this research, we wanted to display the effect of the resonant null, which is signature with passive (signal dissipates in the medium) negative index MTMs. One of the most common experimental analyses used to see this reaction is frequency spectrum measurements shown through scattering parameters (s-parameters) utilizing a programmable network analyzer (PNA). Using s-parameters, we show the resonant behavior and, as discussed in Chapter 2, also derive the impedance (z), as well as effective permittivity and permeability.

Two methods of measuring MTMs were employed. The first testing method is the 10 MHz-4 GHz (0-4 GHz) radio-frequency (RF) stripline as shown in Figure 12. We accomplished 1-D prototype device measurements with the stripline to infer the behavior

of the 2-D MTM structures. 2-D MTM device measurements needed a waveguide structure to measure. Therefore, the BANTAM gave us the opportunity to gather necessary measurements with nearly the same measurement arrangement, while still employing a waveguide structure. Moreover, BANTAM 2-D FBS was designed specifically for measuring 2-D MTMs and supplied a unique opportunity to observe the spatial wave intensities and wave material interactions for each measured frequency using the near-field testing feature.

Figure 12 0-4 GHz Stripline used to measure 1-D metamaterial samples and close-up of sample measurement set-up.

Testing With 0-4 GHz Stripline

The RF stripline measurement arrangement was proven effective for small scale 1-D testing by Langley [10]. Testing with any RF measurement device starts with a calibration. Stripline calibration for these measurements was important because it established the measurement plane and removed error due to cabling connections and empty device space. The calibration plane also establishes the starting point in time for the time domain gating. The calibration standard utilized for these measurements were three different short measurements. These measurements were accomplished with aluminum bars cut to surround the center conductor and touch the top and bottom ground planes when the stripline was clamped down. The bars were placed at three different points along the stripline to establish 12 unique short measurements. Each calibration measurement included a port 1 (forward) reflection and transmission measurements, and a port 2 (reverse) reflection and transmission measurements. An empty line (thru) measurement was accomplished to complete the calibration. These calibration measurements are used to solve the 12 term error model derived from two-port network equation set, with the intention of employing the Nicholson-Ross-Weir (NWR) technique to retrieve the electromagnetic material properties [9] [22] [21].

Testing With BANTAM 2-D FBS

The advantage of using the BANTAM comes from the reconfigurable states of the apparatus. There were three different states intended to use in testing samples: 1) large lens, 2) small lens, and 3) empty. These testing arrangements provided a wide range of information to describe the effects the metamaterial caused. Figure 13 shows the BANTAM 2-D FBS set-up including the control computer and the PNA.

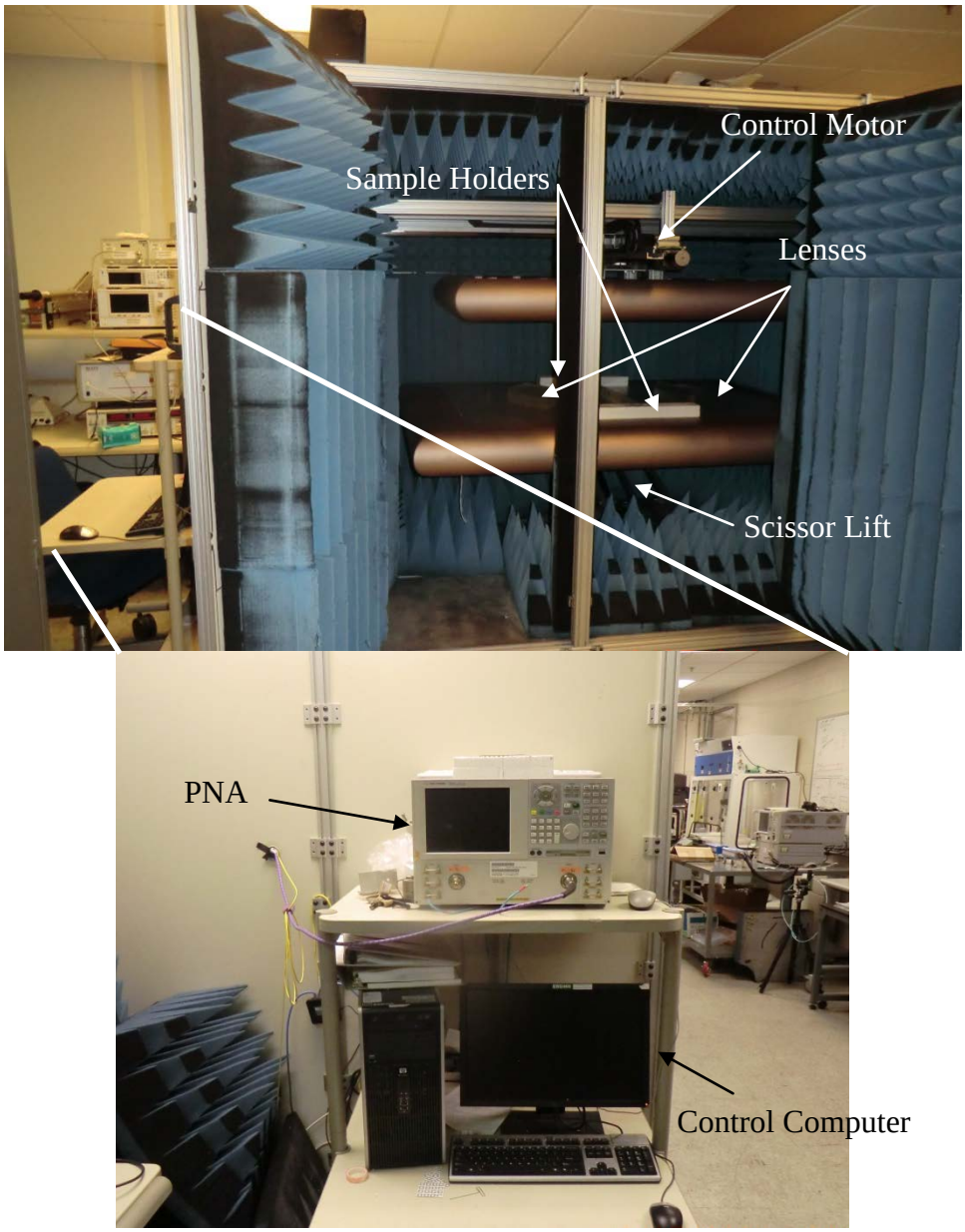

Figure 13 BANTAM 2-D FBS and control system

One of the defining differences in this research as opposed to other research in this area is the use of material property extraction techniques for 2-D MTMs. Specifically, a NWR material property extraction method was used, as described with the stripline earlier. For the BANTAM, instead of two separate pieces clamped around the center conductor, an aluminum bar (the short measurement target) is used to perform the

calibration, based on the 3GHz top frequency. This meant that the spacing was 2 cm in front of and behind the calibration plane. Since the lenses for both the large and small lens measurements are equally spaced away from the center, only the target holder set was used as shown in Figure 13. This calibration technique removed most of the effect of the antennas, the lenses and the free-space in-between the sample and the lenses.

Small lens measurements can include both s-parameter measurements and area scanning measurements (including near-field). The beamwaist of the small lenses is noticeably smaller, about 190.5 mm at the largest, which translates to 19 meta-atom arrays for a complete MTM sample. This configuration allows for scanning in the waveguide by using the alternate connection configuration (connecting the port 2 connection to the top plate antenna connection). Using the scanning configuration, a 381mm x 381mm square centered between the lenses can theoretically be scanned; however, the amplitude tapers off from the beamwaist and across the frequency range. This effect can be seen in Figure 14, which shows an empty measurement separated by frequency.

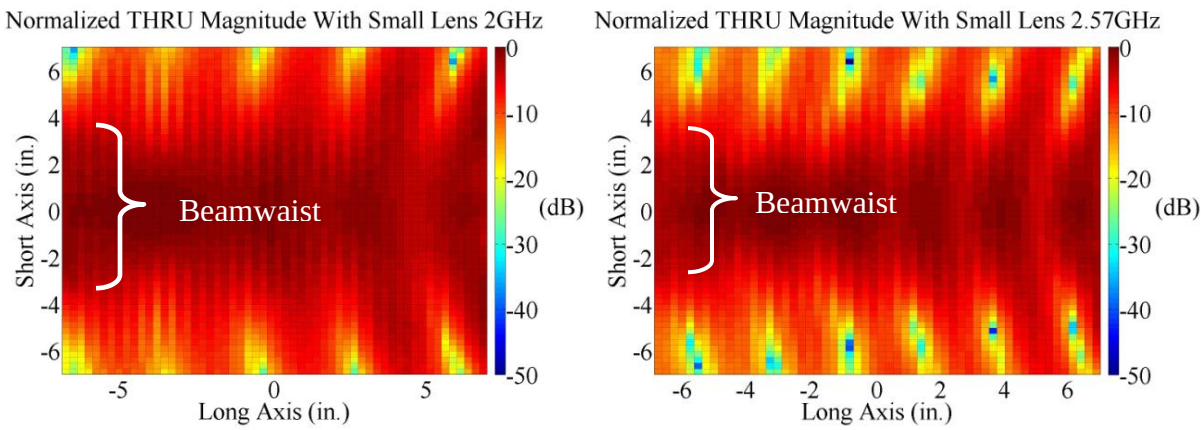

Figure 14 Small lens THRU measurement over a 356mm x 356mm square showing transmission intensities (in dB) at 2GHz (left) and 2.57GHz (right). Also noted is the beamwaist for each frequency which is approximately 7" at 2GHz and 4" at 2.57GHz which is just as described by Faris

To ensure proper working conditions the top conducting plate should rest on the lenses. To accomplish this, the bottom plate is raised until the full weight of the top plate is resting on the lenses. If the bottom plate is raised only to touching the lenses there is always a gap over the right lens. This is not a problem with s-parameter measurements (no movement) or scans within +/-89 mm of the center (along either the long or short axes). However, many near-field scans were accomplished over an area of 356 mm x 356 mm. This scanning area resulted in an issue. The issue arose when the top plate tipped over the edge of the lenses, and once it tipped, the top plate drug the samples and pushed the lenses as it moved which can be seen in Figure 15.

Finally, the last configuration described by Faris was no lens or empty. This configuration was useful to show the direct effect of the MTM on the transmitted signal. Without the lenses in this configuration, the effects from the MTM were apparent. This configuration also gave a better description of how the wave propagates without

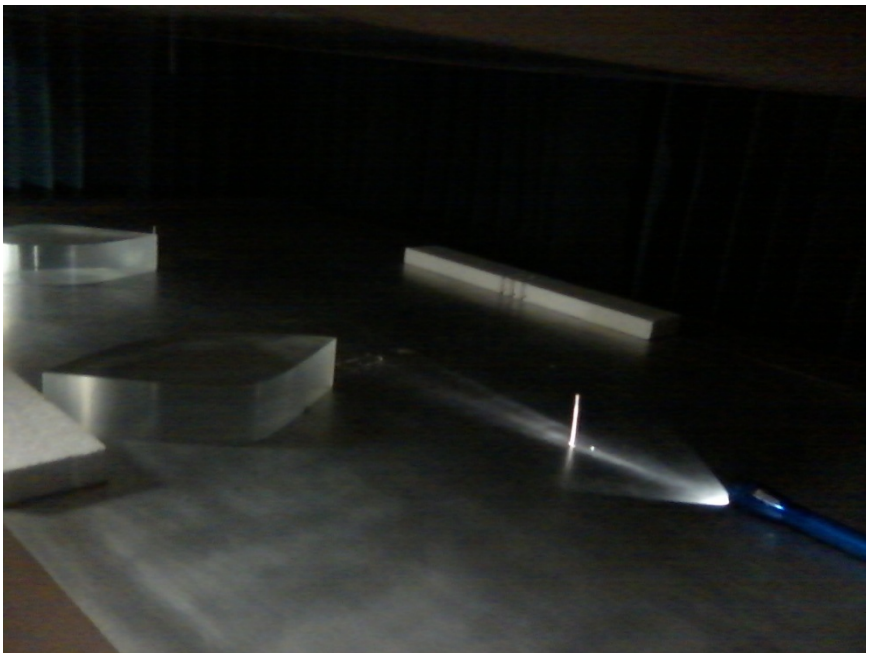

Figure 15 Picture of lenses that were pushed by the top plate.

assistance or hindrance. The complications that arose from higher order TEM modes were also easy to pinpoint with this configuration.

Summary

The BANTAM was verified to be as precise as previously shown. The measurements that follow included small lens s-parameter measurements for material property extraction and small lens near-field measurements for wave-material interactions. Finally, no lens measurements were performed to show the applicability of this metamaterial design and the ability of the BANTAM to measure the reaction.

IV. Experimental Results

This chapter outlines the results from all of the measurements discussed in chapter three. Resonant frequency response experiments for three designs were performed and initial material property calculations are described. These tests helped to choose one design to use when creating a metamaterial. This design was used to create a silver nano-particle ink printed on photo paper meta-atoms for comparison.

Next, the BANTAM 2-D FBS measurements are discussed. The device measurements were centered on two main measurements: a small lens scattering parameter (s-parameter) measurement, and near-field scans without lenses. S-parameter measurements were used to include material property extractions based on an NWR technique as Hanson [22] and Gunn [12] discuss. The second measurement method lends itself to the applicability of this metamaterial (MTM) design. By removing the lenses and surrounding the monopole with the metamaterial in different configurations, we can see the resulting electromagnetic (EM) radiation pattern without interruption and compare it to the empty or non-reactive obstructions for comparison.

0-4 GHz Strip Line Measurements

Stripline measurements used a small sample of meta-atoms and provided a one dimensional result. The stripline measurements also provided the first opportunity to demonstrate the NWR material property calculation method for the two fabrication methods. The measurements to verify the design based on frequency included six measured samples with two at each frequency (because some samples were over-etched). The difference between the two sets of meta-atoms measured is more apparent in Figure 16.

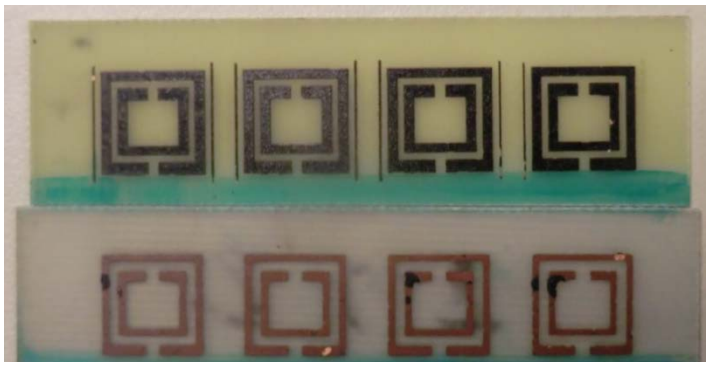

Figure 16 Copper on FR4 etched into 2.5 GHz design. Top is the well fabricated sample and bottom is an over etched sample. The bottom sample has no outer traces and the ring traces are almost half of the width of the other sample.

Resonant Frequency Testing

Table 2 shows results of the analytic model, the simulation model, and the six sample sets that were measured. The analytic model underestimates the measured value by about 15 % (2.06 GHz to 2.42 GHz), which was worse if the traces were considered to be a part of the circuit model (calculated at 3.91 GHz). Conversely, the CoventorWare® simulations overestimated the measured value in most cases, but came closer with only a 4 % (2.82 GHz to 2.74 GHz) difference at worst and .7 % (2.57 GHz to 2.59 GHz which was slightly better than the 2.44 GHz to 2.42 GHz in further precision) at best. These models, therefore, gave a range in which we could expect to see a response.

Table 2 Calculated values are matched with the simulated values, the properly fabricated copper on FR4 samples and the over-etched copper on FR4 samples. All designs are shown relative to the frequency they were designed to meet.

	Analytic	CoventorWare®	Cu on FR4 As Designed	Cu on FR4 Over-Etched
2 GHz	2.06 GHz	2.44 GHz	2.42 GHz	2.48 GHz
2.5 GHz	2.25 GHz	2.57 GHz	2.59 GHz	2.64 GHz
3 GHz	2.31 GHz	2.82 GHz	2.74 GHz	2.80 GHz

As seen in Figure 16, the traces are thinner in the over etched samples. These thinner traces have a decreased inductance which is one of the dominating values in the resonant frequency equation as shown in Chapter 3. Figure 17 shows the measured s-parameters for the 2.5 GHz samples next to each other. In Figure 17 we can see that the over etched sample has a deeper resonant null, but the well fabricated sample has a larger null bandwidth.

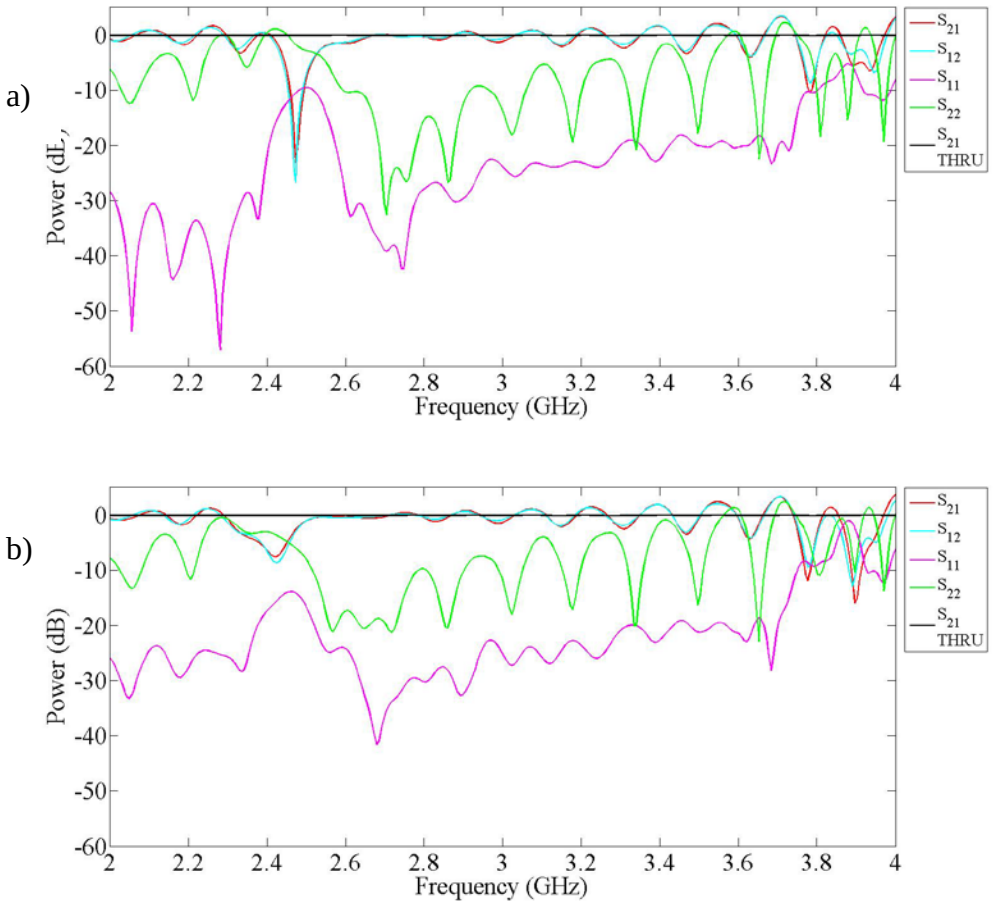

Figure 17 Measured S-parameters for a) over etched sample showing resonant null at 2.68 GHz and forward transmission coefficient (s21) at -30 dB of loss and b) the well fabricated sample showing a resonant null at 2.59 GHz and S_{21} loss of only -9 dB.

The paper meta-atom arrays were then fabricated using the 2 GHz design. This design was chosen to ensure the measurements were within the 2-3 GHz range. The measurement configurations used to test these meta-atoms were designed to display the differences from alignment and spacing of meta-atoms. Tests for alignment used a two array configuration (four meta-atoms to an array). These arrays were measured with one centered evenly or offset above and below the center conductor, and with the metal traces facing opposite directions. Then, to test the effect of spacing on the resonant frequency, four arrays were utilized. Configurations included the evenly centered 10mm spacing and 20mm spacing configurations, as well as metal traces facing each other (instead of all in the same direction). The results are displayed in Table 3. The opposite facing measurement was conducted with the 10 mm spacing and 20 mm spacing; however, there was no difference noted in the resonance frequency with the wider spacing.

Table 3 Resonant points from stripline measurements with silver nano-particle ink printed on photopaper.

2 Sample Arrays	Theory	Centered Evenly	Opposite Facing	Offset
Resonant Point	2.44 GHz	2.95 GHz	3.10 GHz	2.97 GHz
Second Point	--	3.97 GHz	3.90 GHz	3.99 GHz
4 Sample Arrays	Theory	Centered 10 mm	Opposite Facing	Centered 20 mm
Resonant Point	2.44 GHz	2.94 GHz	3.01 GHz	2.96 GHz
Second Point	--	3.92 GHz	3.92 GHz	3.92 GHz
Third Point	--	4.76 GHz	--	4.70 GHz

First, the paper samples consistently had a higher frequency resonance. This could be attributed to two issues: the low dielectric properties of the photograph paper (photo paper), and the thickness of the silver traces. The first theory was tested further by some additional measurements in the metamaterial testing using the BANTAM, which

will be discussed in a later section. The second issue makes sense because it echoes the increased frequency in the thinner traces from over etching in the copper on FR4 samples. The other notable difference was the appearance of multiple resonance points which can also be seen in Figure 18.

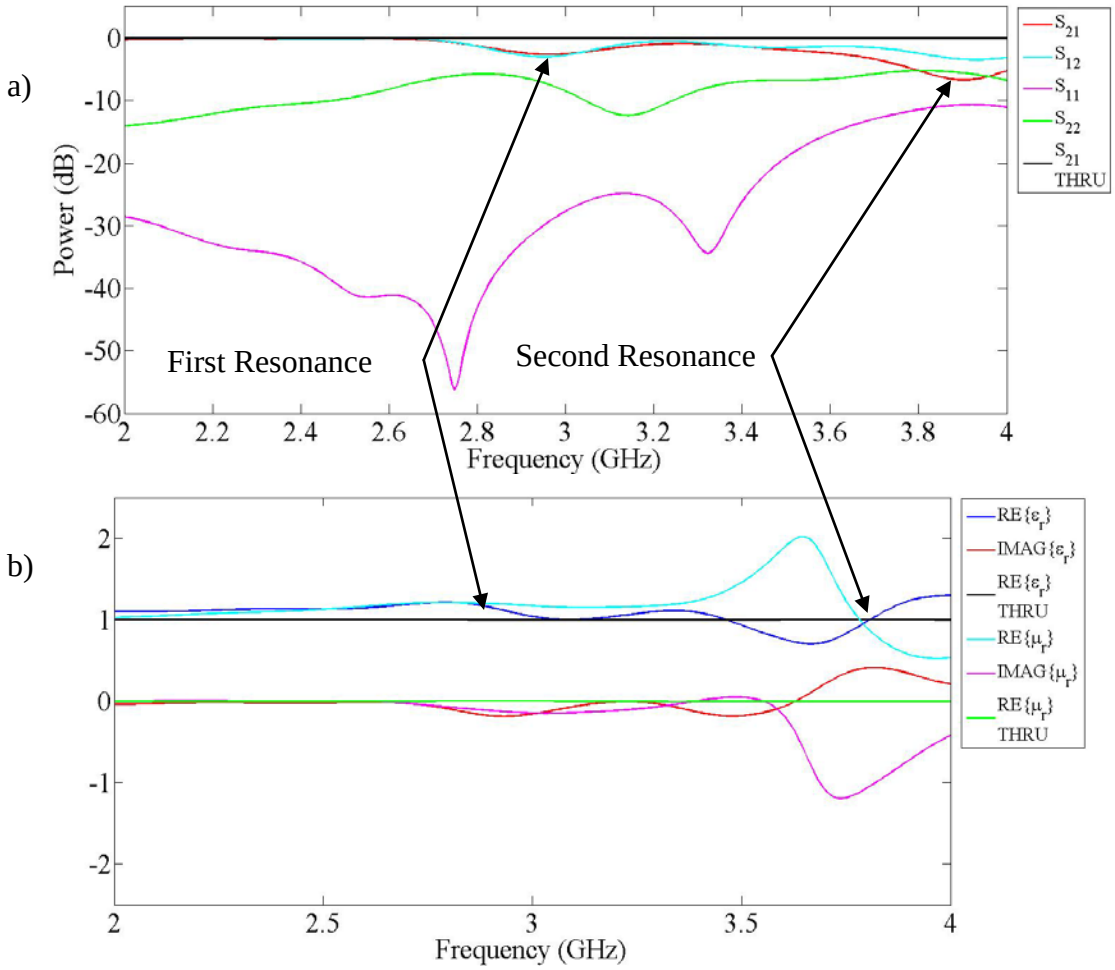

Figure 18 a) Measured S-Parameters for silver nano-ink printed on photo-paper with S_{21} THRU for reference. b) Relative permeability and permittivity extraction and the THRU real permittivity and permeability for reference.

Material Property Extraction

Material property extraction was performed to validate resonant nulls and describe the metamaterial in terms of its relative EM properties. As discussed in Chapter

3, these properties can be used to show the index of refraction, impedance, as well as the relative permittivity (ε_r) and permeability (μ_r). The measured s-parameters of the copper on FR4 measurements and paper samples were used to calculate ε_r and μ_r. Figure 19 and Figure 20 show relative permittivity and permeability for the over-etched 2 GHz design with two meta-atom arrays. The location of the main resonance is at 2.48 GHz because the SRRs were thinner and the traces were completely gone. This also caused an extra resonance at 1.65 GHz and significant reactions above 3 GHz due to the higher order mode interactions.

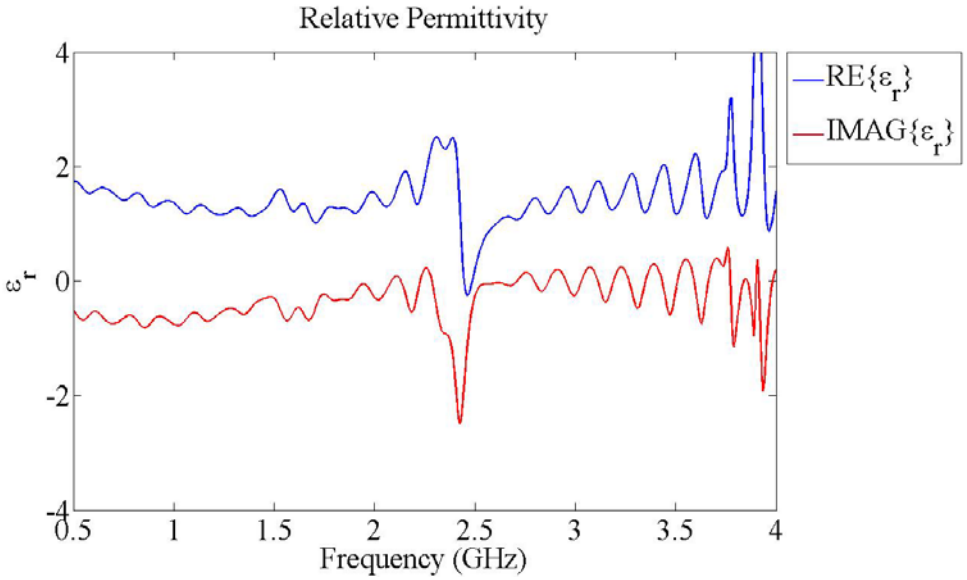

Figure 19 Relative permittivity for 2.48 GHz stripline sample

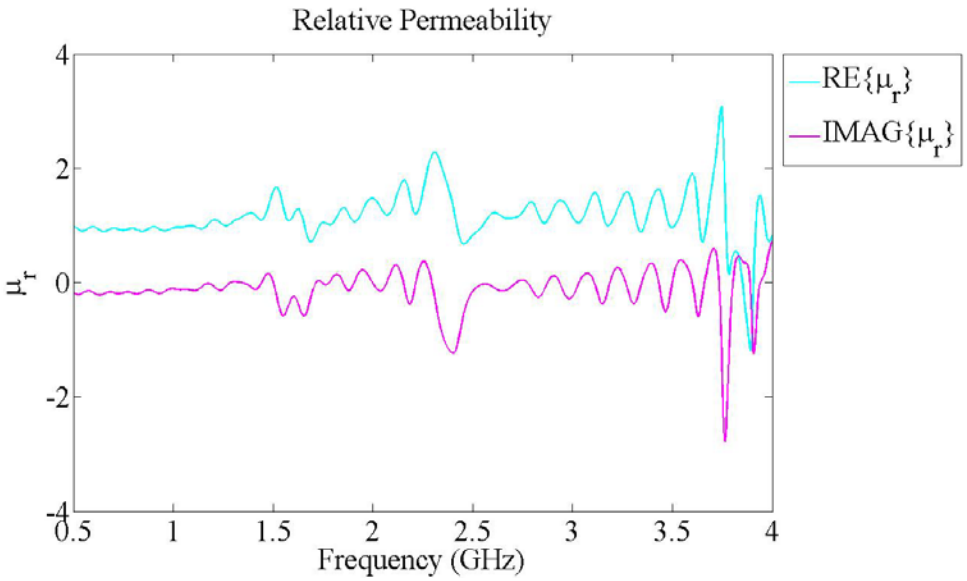

Figure 20 Relative permeability for 2.48 GHz stripline sample

Metamaterial Material Measurements

After the verification measurements were made (discussed in Appendix A), MTM measurements were performed as laid out in Table 4. These tests were s-parameter measurements with the small lenses. For the s-parameter test the three-short calibration method was utilized to remove the reaction of the antennas, lenses, sample holders, and free space up to the metamaterial. Three different material combinations were used with the 2.5 GHz meta-atom design. The materials used were copper on FR4 (CU on FR4), silver nano-ink printed on Epson photo-paper (Ag on paper), and the Ag on paper also backed with plain FR4 (Ag on FR4). Each test was performed with a frequency range of 2-3 GHz and a frequency resolution of 625 KHz (1601 points). The frequency range was utilized to attempt to keep measurements and calibrations within the primary TEM mode.

Table 4 Metamaterial and material property extraction measurement test points

Test Point	Configuration	Description
1	Small Lens	Left-right (THRU)
2	Small Lens	Left-right (Cu on FR4 MTM)
3	Small Lens	Left-right (Ag on paper MTM)
4	Small Lens	Left-right (Ag on FR4 MTM)
5	Small Lens	Left-right (Photo paper)

THRU Measurement (Test Point 1)

The purpose of the THRU measurement that was to verify the three-short calibration technique could calibrate to the center of the testing device accurately. Figure 21 illustrates the three-short calibration for the BANTAM s-parameter measurements and the axes of measurement. The first measurement set after the calibration was the THRU measurements shown in Figure 22. The flat S_{21} and S_{12} were indicative of a good calibration.

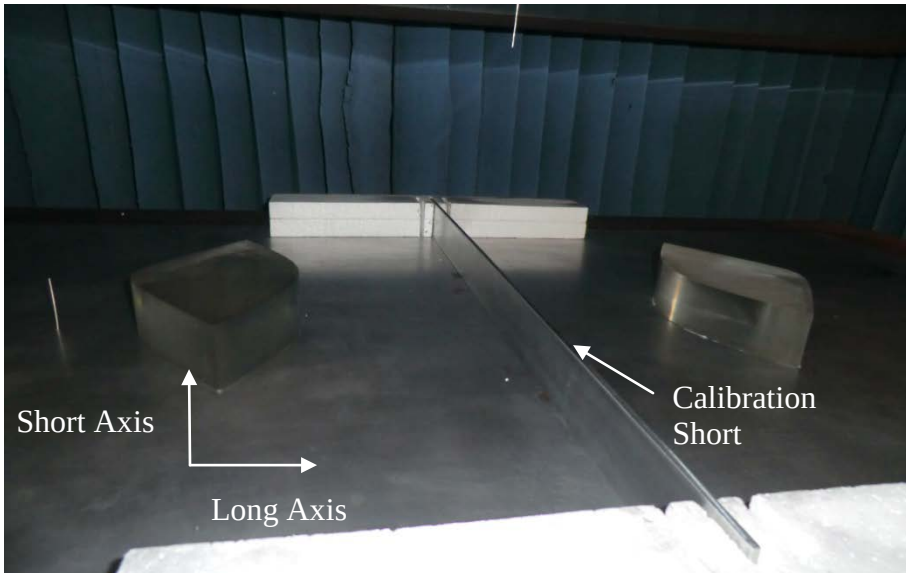

Figure 21 Small Lens three-short calibration for BANTAM

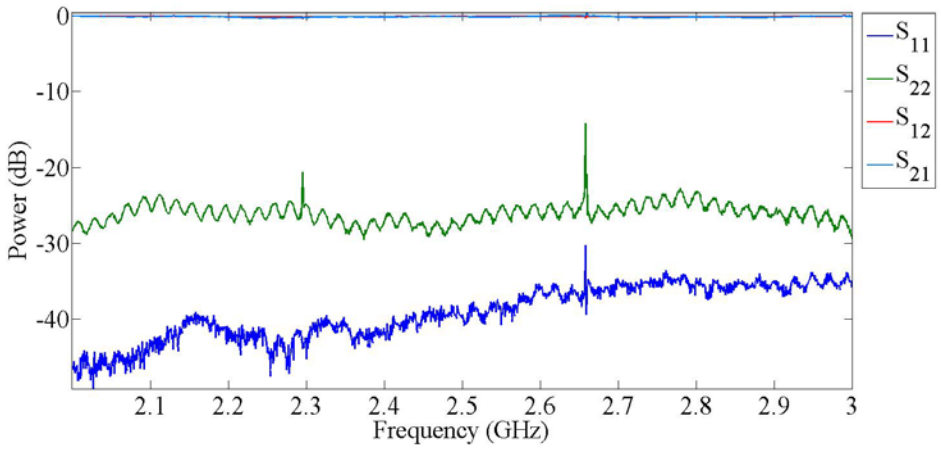

Figure 22 Test point 1 THRU measurement after three short calibration

The ~0 dB transmission is much more indicative of the actual performance of the material within the BANTAM, since there is nothing in between the lenses. The transmission coefficients (S_{21} and S_{12}) indicated a good calibration; however, the noise along the reflection coefficients (S_{11} and S_{22}) shows the need for time domain gating, which, due to the PNA, was applied after measurements were taken. Test points 2-4 were then conducted to show the resonant null and retrieve the relative EM material properties.

Metamaterial Measurements (Test Points 2-4)

The purpose of the s-parameter measurements was to test the viability of the BANTAM for use in material property extraction. The measurements were all performed within the 2-3 GHz range. This range was chosen in order to stay within the fundamental mode to utilize the NRW material property extraction. Frequency resolution was set to 1 MHz, and the calibration here was the same as the stripline using the three-shorts and a THRU measurement. The benefit of this setup is that calibration plane becomes the measurement plane instead of the monopoles.

Due to the findings shown in Appendix B with the large lens measurements, the MTM was constructed for the small lens measurements. To be more comparable to the stripline measurements, the samples were cut down to sections of 4x4 meta-atoms. These smaller sections were slotted into a low density foam sample holder with 10mm spacing between samples shown in Figure 23. Due to the limited number of MTM sections, the holder was designed to hold a maximum of 17 samples and was about 170 mm wide. The sample holder only left out one 4x4 meta-atom array from the original MTM layout and took up almost the entire 178 mm beam width of the small lenses. Therefore, the small lenses were chosen to perform the s-parameter measurements over the large lens measurements for all of the metamaterial samples.

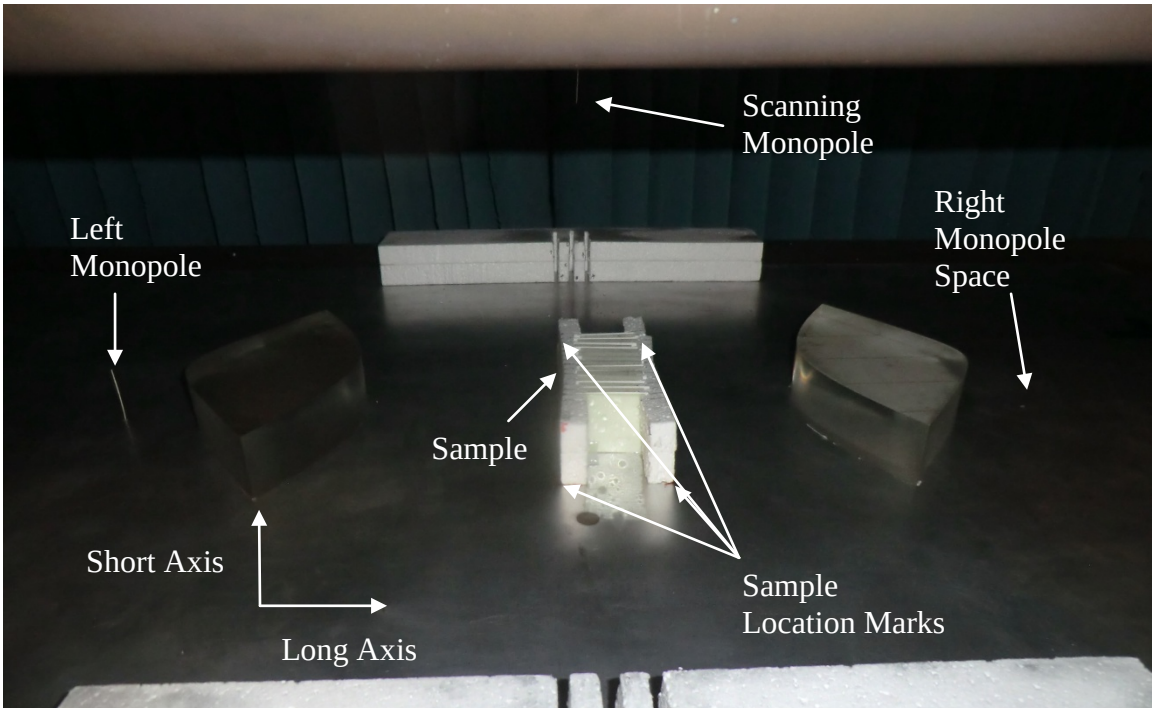

Figure 23 Pictured here is the material measurement sample set-up for near-field "block" measurements. The s-parameter measurement set-up differs only with the right monopole instead of the scanning monopole.

Figure 24 shows the forward transmission for the metamaterial samples which indicate a resonance just like the associated stripline measurements. For each of these measurements 625 KHz frequency resolution (1601 points) was used so they could be compared to the stripline measurements. Figure 24 also shows that the photo paper (test point 5) did not incite any noticeable effect. When compared side by side, the silver on photo paper MTM (test point 3) has the widest bandwidth response (starting at 2 GHz and continuing past 3 GHz) but a lesser depth of null (only -9.54 dB of loss). However, when a stronger dielectric substrate is utilized we can see that the bandwidth is still good (2.25 GHz to 2.92 GHz) with the silver on FR4 (test point 4). However, the null is also deeper (~-22dB as opposed to ~-18.5 dB) than the copper on FR4 (test point 2), which was expected because of the better conductivity of the metal.

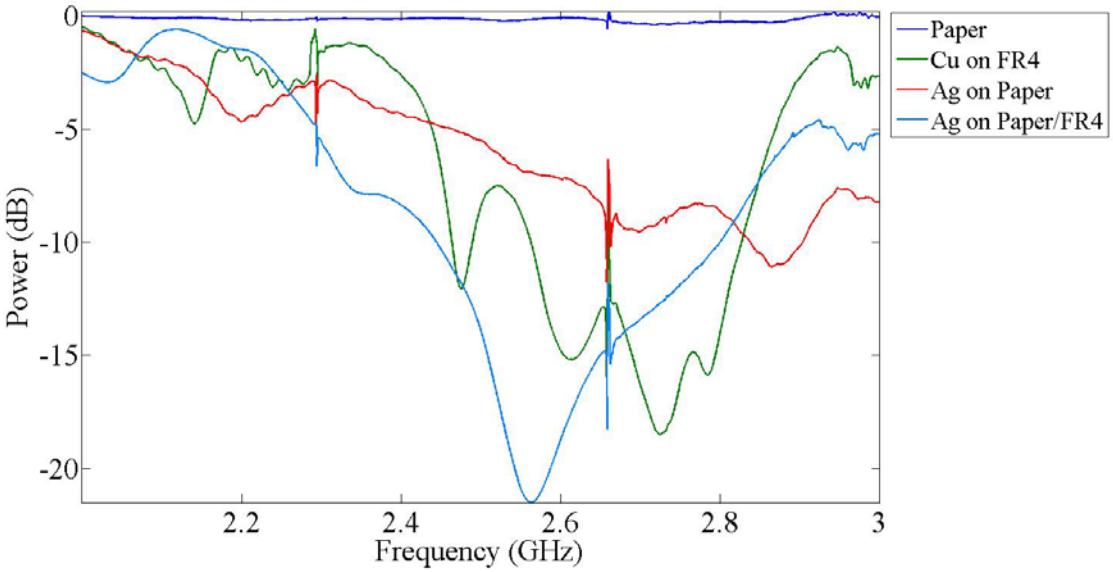

Figure 24 Forward transmission for all metamaterial samples and plain photo paper

The most interesting effect shown throughout these measurements is the shift in the center of the resonant null. From Figure 24 we can get the deepest measured resonant nulls, which are captured in Table 5. The highest frequency resonant null belongs to the

silver-based MTM (2.86 GHz). This is because the paper provides no barrier between the silver SRR meta-atoms. The coupling then increases the frequency, as described previously with the stripline measurements.

Table 5 Resonant null from metamaterials measured in the BANTAM with the small lens set-up.

Metamaterial	Resonant Null (GHz)	Loss (dB)
Ag on Photo Paper	2.86	-11.08
Cu on FR4	2.72	-18.48
Ag on Photo Paper and FR4	2.56	-21.75

The material property extraction did not present as expected as Figure 25 shows. Figure 25 shows the relative permittivity and permeability of silver on photo paper with FR4 with the real parts of the THRU permittivity and permeability for reference. This sample showed the best resonant null; however, the relative EM properties were far from stable. Figure 25 suggests that these samples stimulated several resonances across the entire frequency range of interest. Unfortunately, they overlap significantly, so it is difficult to separate the individual nulls. However, at least three nulls are easily seen.

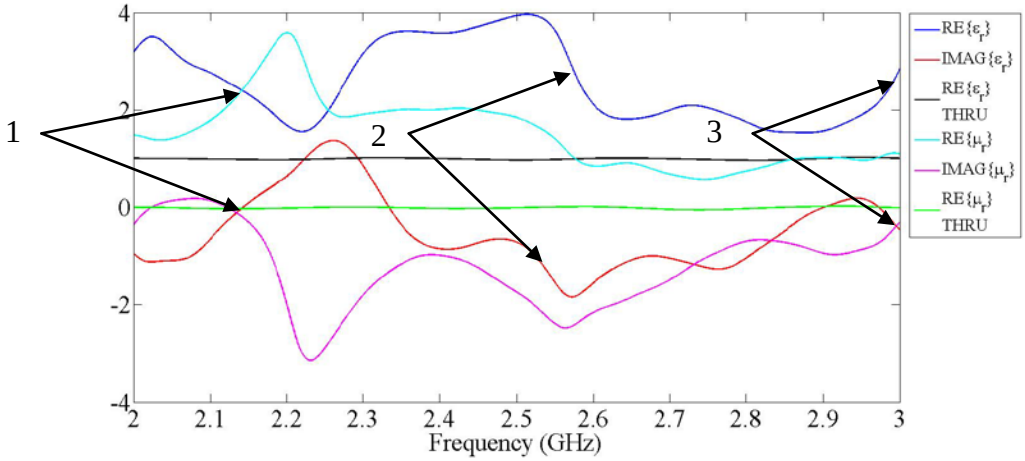

Figure 25 Extracted relative permittivity and permeability for the silver on photo paper with FR4 backing with the three most likely resonant nulls labled

Metamaterial Near-Field Measurements

The near-field measurements are performed by scanning throughout the PPWG and taking field measurements. The purpose of these measurements was to characterize the applications for this design and demonstrate which materials performed best for each design intention. First, with the small lens, the MTM was placed in the center and a front and rear scan was accomplished to show block possibilities (e.g. signal absorbing surface, reflector, or lens). Second, we removed the lens and tested two configurations without the lens to showcase possible applications for this design.

Table 6 Near-Field Scanning Test Points

Test Point	Configuration	Description
1	Small Lens	Left Monopole (THRU)
2	Small Lens	Left Monopole (Photo paper)
3	Small Lens	Left Monopole (Cu on FR4 MTM)
4	Small Lens	Left Monopole (Ag on paper MTM)
5	No Lens	Left Monopole (THRU)
6	No Lens	Left Monopole (Blocking)
7	No Lens	Left Monopole (Focusing)

Small Lens Measurements (Test Points 1-4)

The two main materials used for comparison were the copper on FR4 and the silver on photo paper. The THRU measurement was used to show the baseline field without interference and ensure a good calibration and measurement setup. The two other measurements were added due to the reduced reactions from the silver on photo paper meta-atom measurements (test point 4) to see if the FR4 added to the paper would affect the response due to the higher relative permittivity reducing the coupling between meta-atoms.

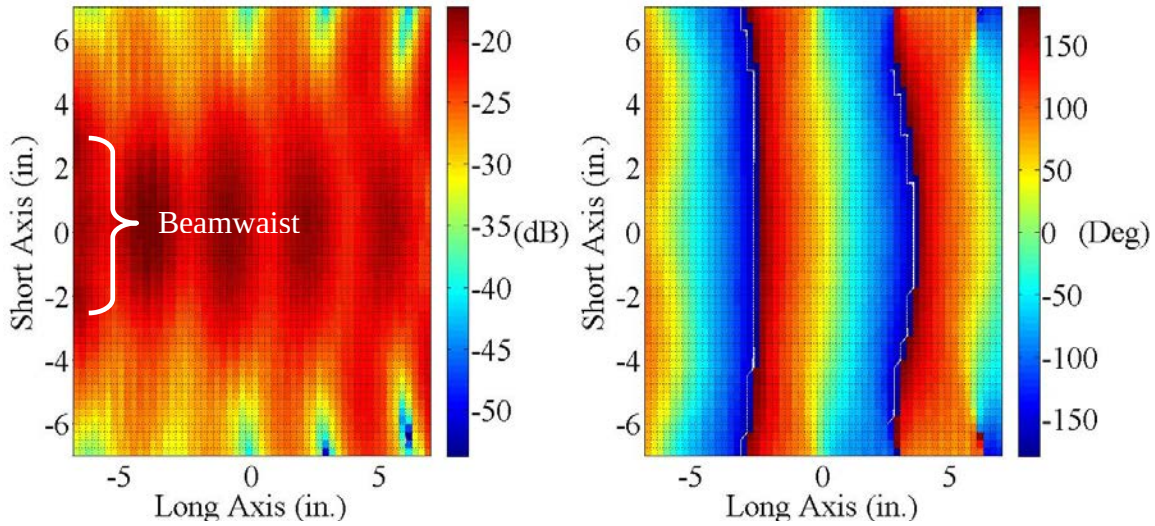

Figure 26 Small Lens THRU measurement magnitude and phase at 2GHz

The THRU measurement was performed before each calibration, and Figure 26 shows a sample of test point 1, the THRU near-field scan with the small lenses. The frequency resolution used was 10 MHz (101 points) to have a similar frequency resolution to the 2-18 GHz case. A scanning area of 356 mm x 356 mm was used with a spatial resolution of 6.35 mm in both directions. This large area was utilized to ensure the entire beamwaist was within the scanning area and to verify the center and width of the beamwaist.

The beamwaist can be seen at the center with a width of about 179 mm, as described previously. Some phase distortion can be seen near the edges; this is due to some reflection off of the receiving lens surface. These also matched the verification tests performed and the measurements reported by Faris [8].

The material measurements posed a dilemma. Figure 27 shows the 2.72 GHz magnitude and phase plot (front and rear) from test points 3, the small lens near-field measurement of Cu on FR4 metamaterial. This was selected based on the previous s-

parameter measurements to showcase where the resonant null was shown. These measurements were accomplished in an area 12.7 mm x 179 mm in front of and behind the sample. The resolution away from sample was 2.54 mm and a resolution of 6.35 mm across the sample. Figure 23 showed a sample setup for this configuration inside the BANTAM.

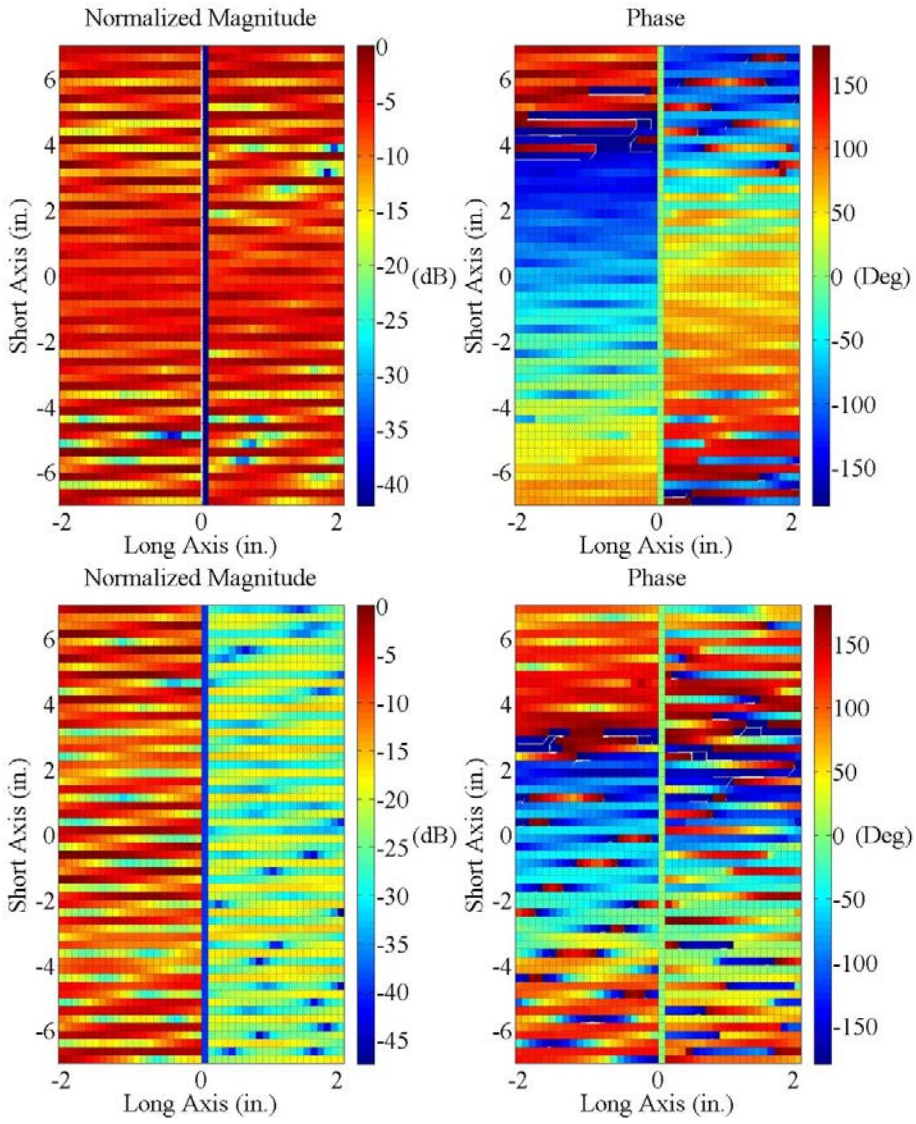

Figure 27 Response for copper on FR4 MTM at a) 2 GHz and b) 2.72 GHz. Both front and rear of material shown and the positive distance is relative to the back of the MTM

The samples were placed in the center and carefully aligned between the lenses to get the highest intensity effect from the lens focusing. The corners of the sample holder were placed within marks on the bottom PPWG plate to ensure that the samples were all measured the same in as shown in Figure 23. The two MTM samples had some similar performances for this configuration.

The differences that were observed can be matched to the s-parameter measurements shown in Figure 24. As seen in Figure 27, the left for 2 GHz is about the same as the right (normalized average power on the left of -8.05 dB and on the right it is -7.04 dB), but at the resonant point the right is 4 dB lower with a normalized average power of -11.06 dB. However, at 2.63 GHz the left is 3.68 dB higher than the right, alluding to the high reflection, without the absorption from the resonant null. The Ag on paper absorption effect is from 2.45 GHz to 2.57 GHz, whereas the Cu on FR4 is from 2.49 GHz to 2.54 GHz; but the absorption increases again at 2.68 GHz throughout the rest of the frequency range. Figure 28 summarizes these differences across the entire frequency range.

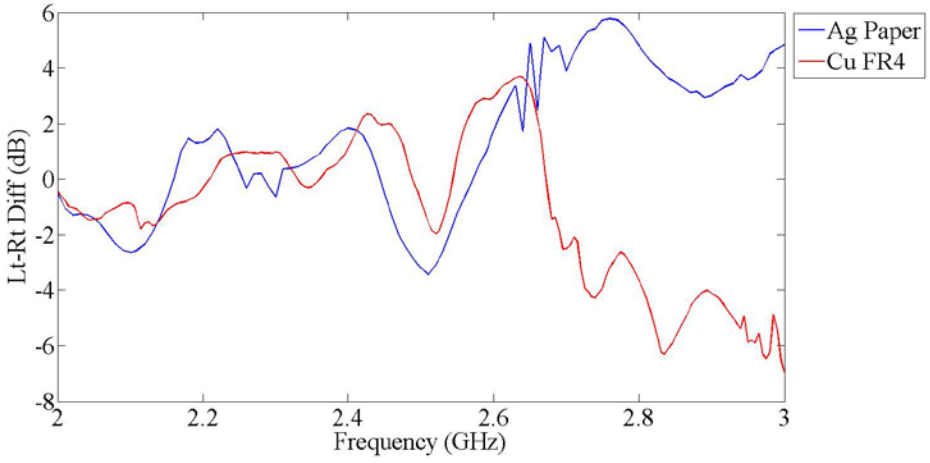

Figure 28 Average power difference between the left side (closest to transmitter) and right side (side furthest from the transmitter)

In Figure 28 the average power on the right (side furthest from the transmitting antenna) is subtracted from the average power on the left (the side closest to the transmitting antenna). Figure 28 shows us that the main resonance for both MTMs is about the same at about 2.5 GHz where they are absorbers. The difference is after 2.64 GHz where the Cu on FR4 becomes an absorber and the Ag on paper becomes reflective. This effect is mimicked in the application measurements, where the Ag on paper shows better results with the focusing arrangement, and the Cu on FR4 presents better in the absorber arrangement.

No Lens Measurements (Test Points 6-7)

Measurements without the focusing lenses provided a near free space environment in which to test the MTM. This testing configuration was also used to display the effect of surrounding the monopole in different configurations. The configurations surrounding the monopole were designed to highlight the reflection and absorption effects of the MTM at the resonant frequency.

Similar to the small lens measurements a THRU measurement was accomplished to verify a good calibration and provide a baseline for the following measurements. The scan area for this measurement was 356 mm x 356 mm with a spatial resolution of 6.35 mm. The frequency resolution used was 10 MHz, which was the same for both test points (blocking transmission with both MTM types, and focusing with both MTM types). Figure 29 shows a no lens THRU measurement, which matches those done in the verification measurements and those reported by Faris [8].

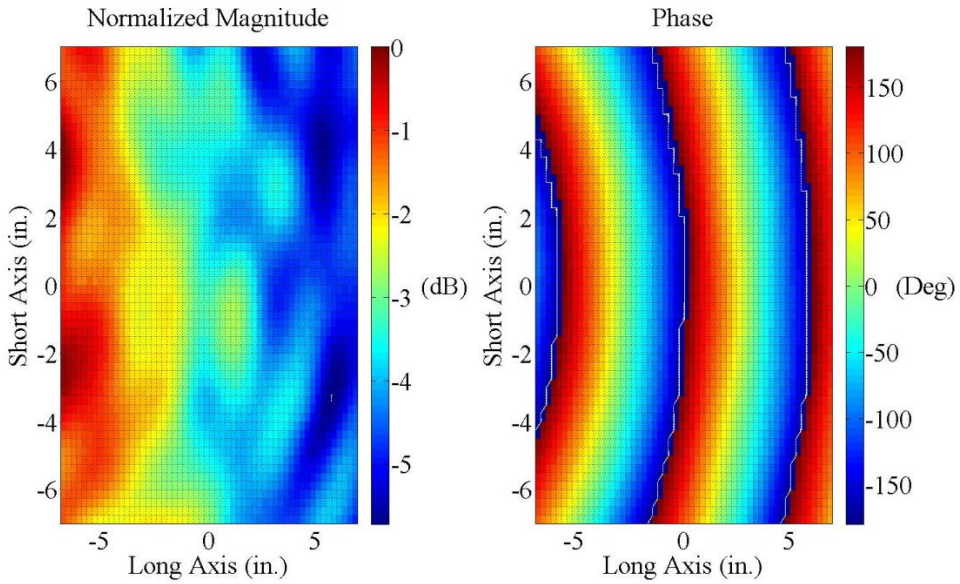

Figure 29 2 GHz normalized magnitude and phase from a no lens THRU measurement

The free space loss is only 6 dB at most across the measurement space, and the phase response pointed to the proper frequency. The two test points 6 (blocking) and 7 (focusing) surround the antenna to highlight the effects that the MTM could provide when directly interacting with the source. The blocking arrangement was created by placing the MTM in a starburst pattern as shown in Figure 30 to provide the best chances for blocking the output power across the PPWG with the available number of meta-atom arrays. Test point 8 was arranged like a corner reflector as shown in Figure 31 to force the power along the direction of propagation. For each test point, Ag on paper and Cu on FR4 were tested as well as Ag on FR4 for comparison.

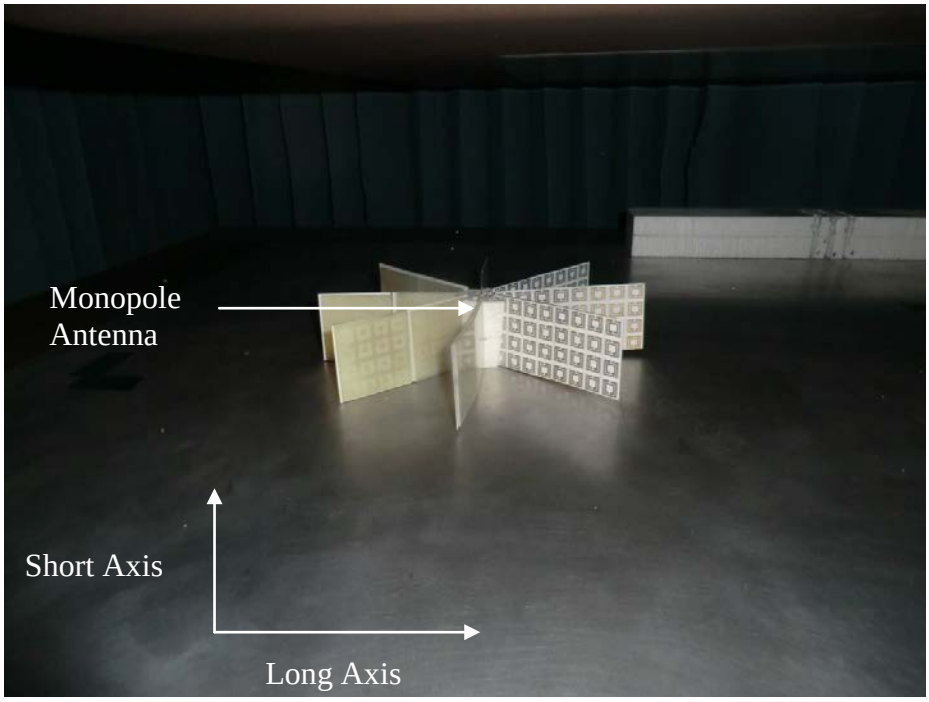

Figure 30 Blocking set-up showing silver on photo paper with FR4 backed MTM

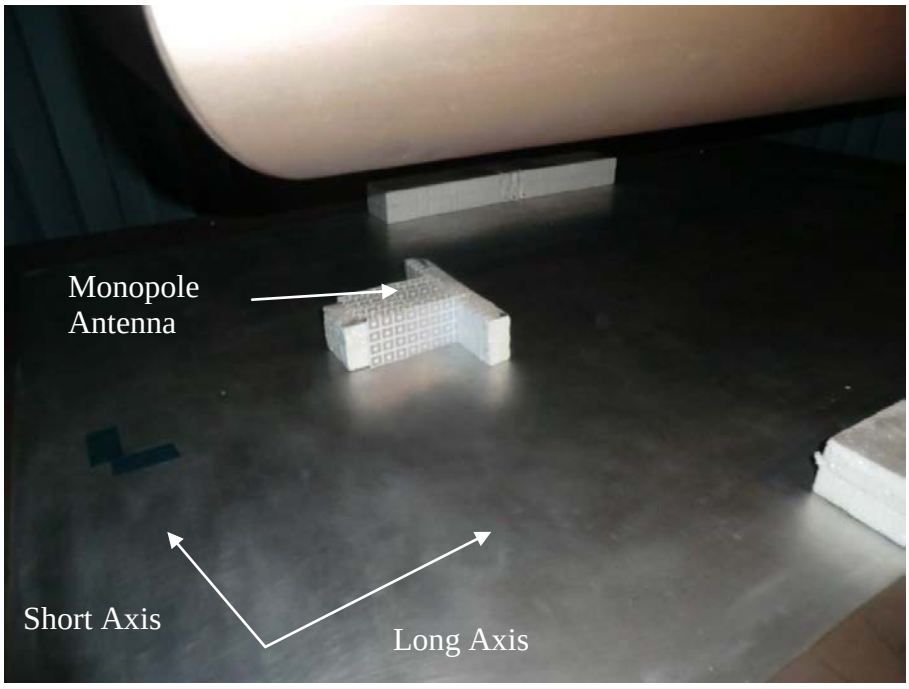

Figure 31 Focusing configuration for no lens measurements showing silver SRR on photo paper backed with FR4 MTM

Each metamaterial blocked the output power differently and at different frequencies. The silver on photo paper started to show some blocking at about 2.67 GHz with the peak effect occurring at 2.86 GHz with a peak loss of -57 dB and the effect continued past 3 GHz (with peak losses greater than -10 dB) spreading to the sides as shown in Figure 32. Figure 32 shows the 2.85 GHz magnitude and phase. Just like the centered measurements, the phase becomes severely distorted, which contributes to the low intensity by providing out-of-phase waves.

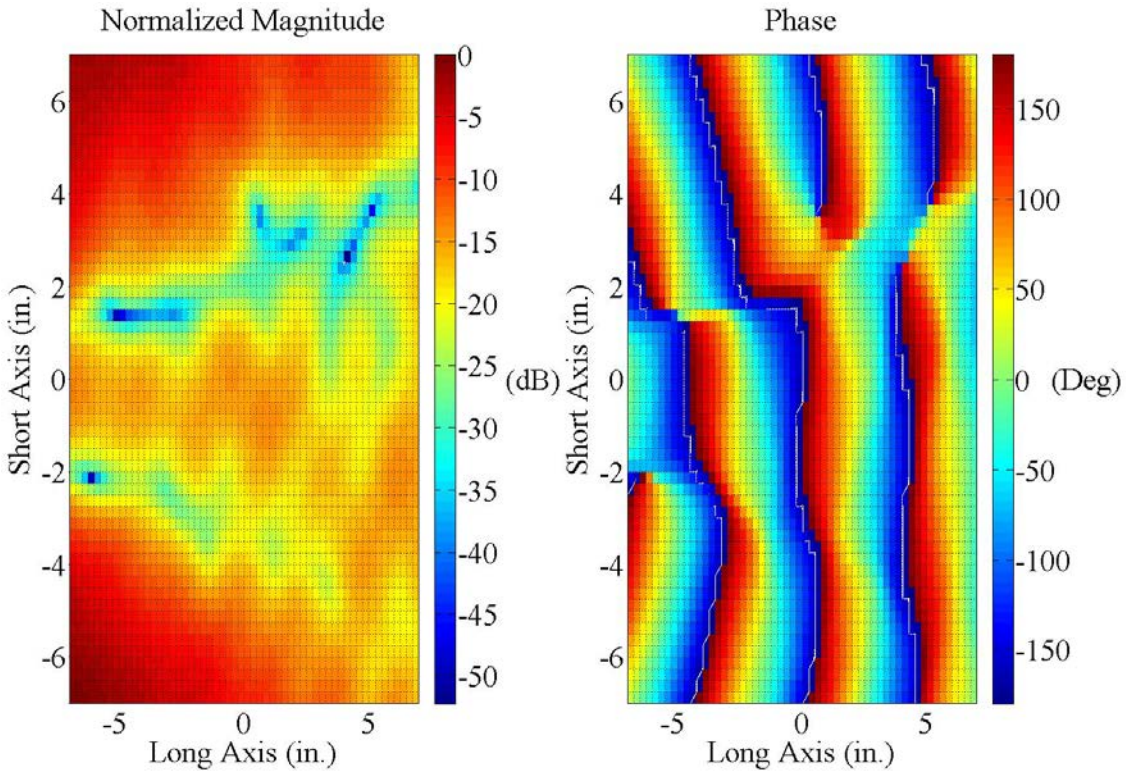

Figure 32 2.86 GHz blocking configuration silver printed on photo paper MTM

The copper on FR4 MTM shows some blocking at 2.68 GHz (~-10 dB of loss) with a peak reaction at 2.75 GHz (-41.8 dB of loss). This reaction only occurs up to about 2.9 GHz (this was the last point with greater than -10 dB of loss). The difference with this MTM is that the reaction often occurs off to one side or the other, as opposed to the

Ag on paper MTM which was more forward focused. This reaction was also seen when the Ag on paper MTM was backed with FR4.

Figure 33 shows the Ag on FR4. Unlike the Ag on paper which reacts over a range greater than 330 MHz (2.67 GHz to >3 GHz) the Ag on FR4 reaction occurs over 270 MHz (2.48 GHz to 2.75 GHz) which was more than the 220 MHz (2.68 GHz to 2.9 GHz) from the copper on FR4. Although, unlike the other two MTM measurements the null was both deeper (-59 dB) and more aligned directly down the center of the measurement area as seen in Figure 33. This reaction was probably due to a combination of the higher conductivity metal and the high relative permittivity dielectric preventing the meta-atoms from having a large coupling effect.

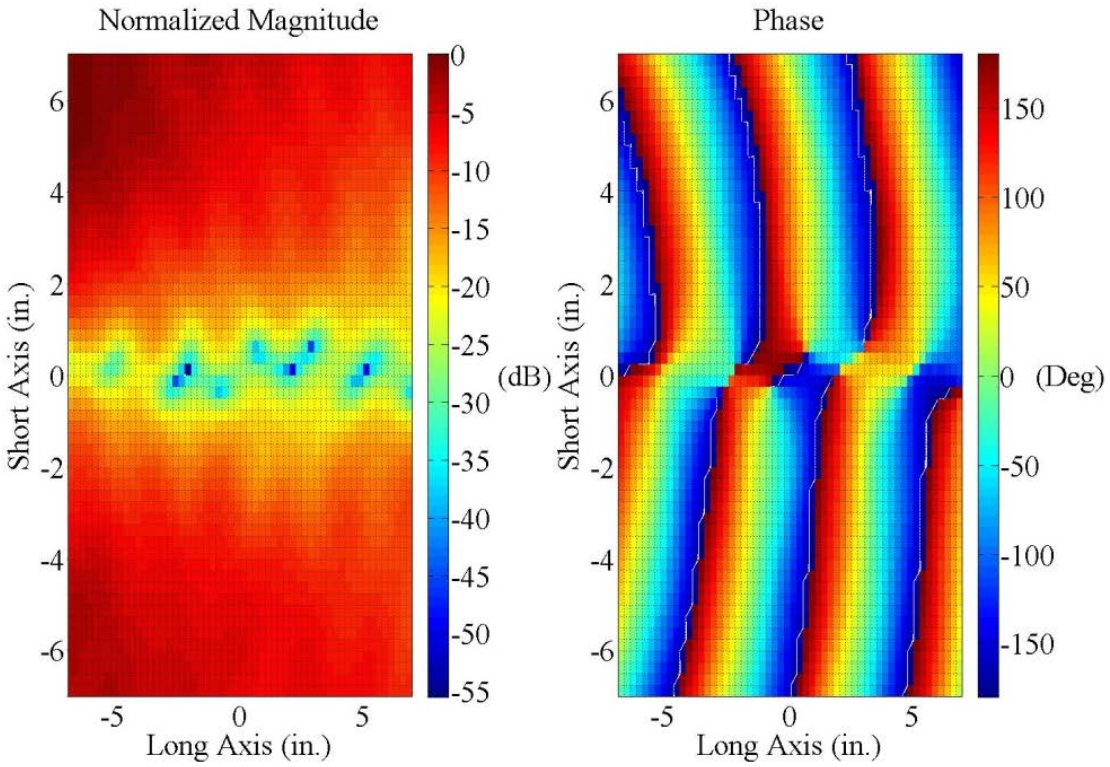

Figure 33 2.70 GHz blocking measurement for silver on photo paper with FR4 backing

Test point 8 (focusing) provided a counter point to the blocking configuration by attempting to focus the output power. Unlike the blocking configuration, the results were skewed in favor of the FR4 backed MTM samples. The copper on FR4 MTM showed the focusing effect between 2.61 GHz and 2.81 GHz with a maximum focusing at 2.74 GHz with only 5 dB loss across the measurement area as shown in Figure 34. The Ag on FR4 had no more than 5 dB loss across the measurement area with the best focusing at 2.79 GHz with only 3.5 dB of loss across the measurement area. As Figure 28 suggests the Ag on paper had the lowest transmission loss across the measurement area with only ~2 dB of loss at 2.61 GHz. However, due to the magnitude coming from the power being reflected from behind the transmitting antenna the phase becomes distorted as shown in Figure 35. This effect only becomes worse as the frequency increases as the reflections become destructive interference.

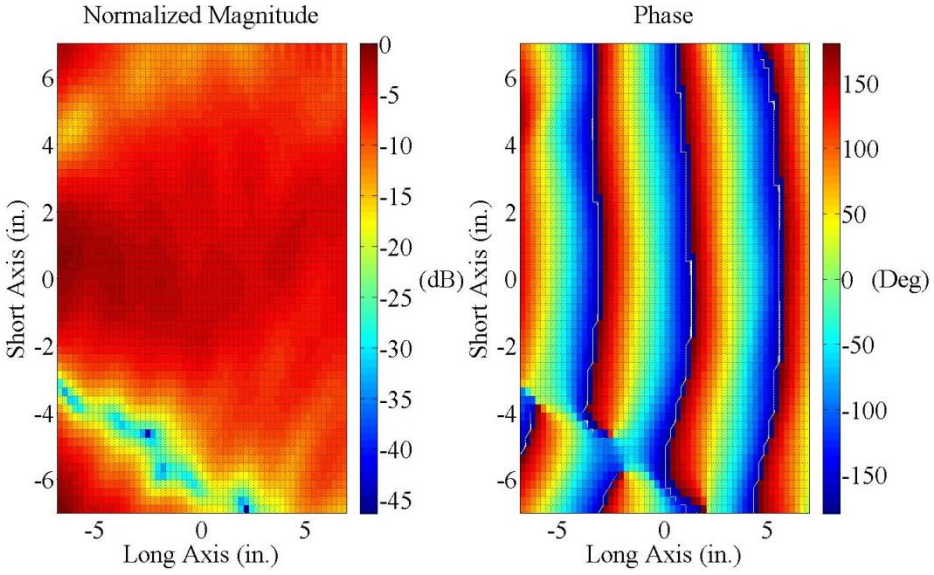

Figure 34 Focusing configuration for Cu on FR4 MTM at 2.74 GHz measured without focusing lenses

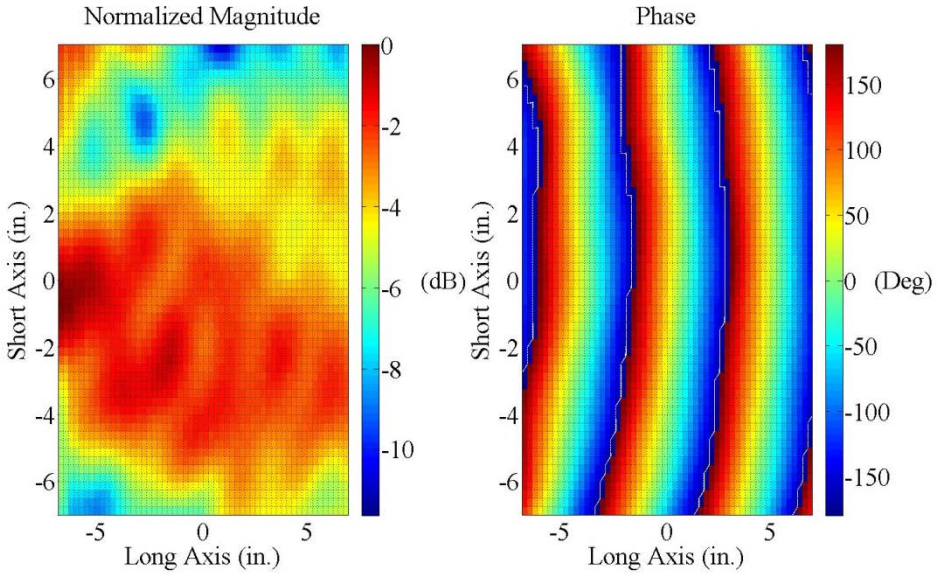

Figure 35 Focusing configuration for Ag on paper MTM at 2.61 GHz measured without focusing lenses

V. Conclusions and Recommendations

Conclusions from Results and Analysis

We have designed, fabricated, and tested a metamaterial structure with two different fabrication methods. During testing this work, we showed successful extraction of constituent electromagnetic material properties with both the 1-D meta-atom measurements and metamaterial measurements, with some difficulties to be noted. We also successfully applied this design to create a frequency blocking device and a focusing device. Each test performed showed some aspect of the metamaterial and added to the description of the final performance.

The three main tests we performed included: 1) 1-D meta-atom stripline s-parameter measurements, 2) BANTAM 2-D FBS metamaterial s-parameter measurements, and 3) application based near-field scanning. Each type of test performed a role in the metamaterial design and testing process. Stripline testing provided a good allusion to complete performance of the metamaterial and verified the design to resonance frequency; these tests showed that they could not describe the actual performance because of the coupling that would occur between meta-atoms in close proximity. The BANTAM s-parameter measurements gave the first description of how the metamaterial performed. We could see the loss in transmission and high reflection in the same area, so two applications became apparent, one for blocking signals (high loss of transmission), and one for focusing signals (high return reflection).

Measurements indicated the highest performing MTM was the silver meta-atoms printed on photo paper with FR4 backing. These devices performed closest to modeling, with a resonance within .4% of the simulated value (2.56 GHz measured and 2.57 GHz

simulated). Ag on FR4 also gave the best resonance at -21 dB for measured the s-parameters, which was 3 dB more loss than the common Cu on FR4.

The device, however, had severe reliability issues (with some batches) that lead to difficulty in gathering coherent measurements. Delamination of the silver was the biggest problem with the printed devices, which was inconsistent between fabrication runs. The other problem (solved with the FR4 backing) was the low dielectric value of paper. Since the devices couple by proximity, having a high relative permittivity substrate was important to ensure performance where we expected it. We saw that without the FR4 backing the resonance is poor (-11 dB as opposed to -21 dB with the FR4) and at a much higher frequency than expected with the null measured at 2.86 GHz, which is 11.3 % greater than the CoventorWare® simulations at 2.57 GHz.

Recommended Follow on Actions

To assist in good material property extraction, the scissor lift needs to be updated to allow for a more even bottom plane. When in full compression the right lens tends to have a gap and as the top plate scans for near-field scanning it tends to lean over the edges of the lenses causing lens drift and crushing material edges.

We suggest either a better lift or a more robust method of keeping the lenses in place. An acrylic or rexolite lens holder for the corners of the lenses would have a minimal impact, and would benefit the system by reducing the time spent aligning the lenses; it would also stop the problem of lens drift for near-field scanning. More fixed sample holders would also be helpful, as the low density foam holders tend to wear out after 4-5 measurements and need to be measured and cut by hand for the samples.

Previously suggested by Faris, creating octave lens sets to have a higher frequency fundamental mode would be beneficial to any material property experiments in the future. These lens sets would also need matching antennas and it is this author's recommendation that monopoles are good enough for most measurements with this equipment.

Recommendations for Future Work

Two avenues could be followed from this work. The first would be material property extraction testing with other dielectrics, and metamaterial designs which should include the higher frequency calibrations actions. The second would be to measure different designs of metamaterials to increase the available applications. This line of research could also include more applications such as beam steering, signal blocking (to assist in multiple antenna scenarios), and active elements to increase the resonance or change the frequency of resonance.

Appendix A

BANTAM 2-D FBS Characterization Tests

To be assured of the viability of the BANTAM a sample of the measurements Faris outlined were performed. Table 7 outlines the measurement sets performed which included the small lens measurements, large lens measurements and the empty parallel plate waveguide (PPWG) configurations. The lens measurements were conducted with the complete 2-18 GHz range as described by Faris [8]; however the empty PPWG measurements were only performed for the measurement range of interest (2-3 GHz).

Table 7 BANTAM Verification Tests

Test Point	Configuration	Function	Description
1	Small Lens	Near-Field Scan	Left Monopole (THRU)
1	Small Lens	Near-Field Scan	Left Monopole (D-Rings)
2	Small Lens	S-Parameters	Left-right (SHORT)
3	Small Lens	S-Parameters	Left-right (Acrylic)
4	Small Lens	S-Parameters	Left-right (D-Rings)
5	Large Lens	S-Parameters	Left-right (THRU)
6	Large Lens	S-Parameters	Left-right (SHORT)
7	Large Lens	S-Parameters	Left-right (Acrylic)
8	Large Lens	S-Parameters	Left-right (D-Rings)

Small Lens Measurements (Test Points 1-5)

Near-field scans for the small lens configuration included two sets: THRU and the D-rings sample. Scanning measurements were from the left monopole to the top probe after cable end calibration. As discussed in Chapter 3 the calibration set for these measurements were short, open, load and thru (SOLT) to the cable ends before the antenna connections. S-parameter measurements were taken from left to right monopole and calibrated in the same way as the near-field scans.

Near-Field Scans

These measurements were accomplished over the 2-18 GHz frequency range with 20 MHz resolution (801 points) within a 356 mm x 356 mm scanning area using 6.35 mm spatial resolution. For comparison, Figure 36 (2 GHz) and Figure 37 (6 GHz) show the measurements performed respectively with those previously reported. No significant differences could be noted for either case with the crest to crest phase difference matching the correct frequency measured.

a)

b)

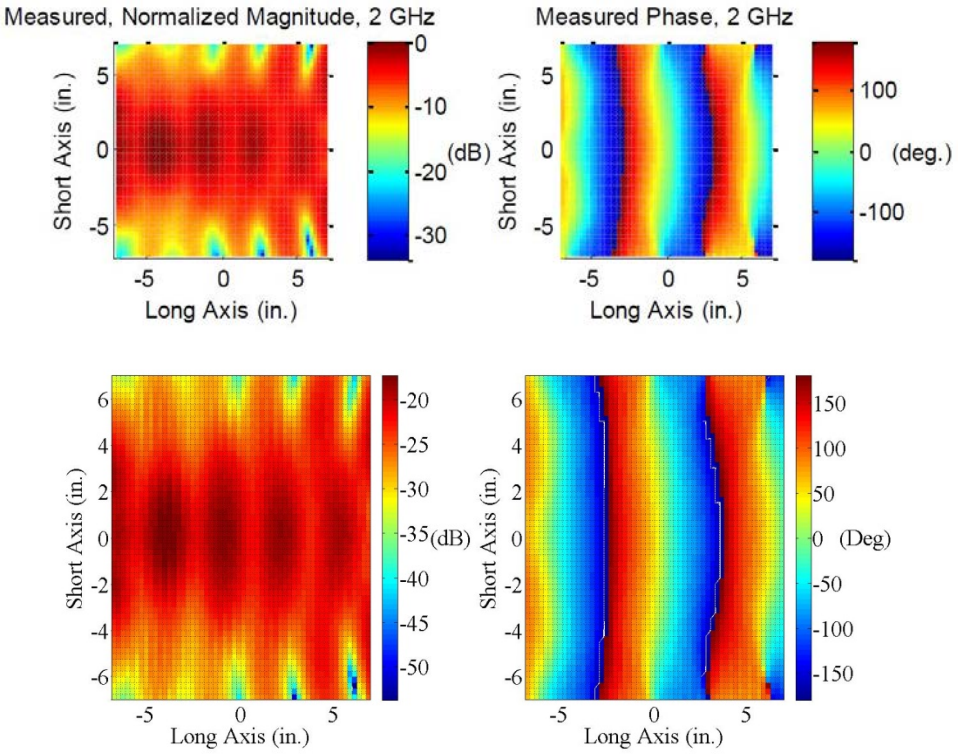

Figure 36 a) Measured (not normalized) THRU magnitude and phase for 2 GHZ with small lens b) reported measured (normalized) magnitude and phase for 2 GHz with small lenses [8].

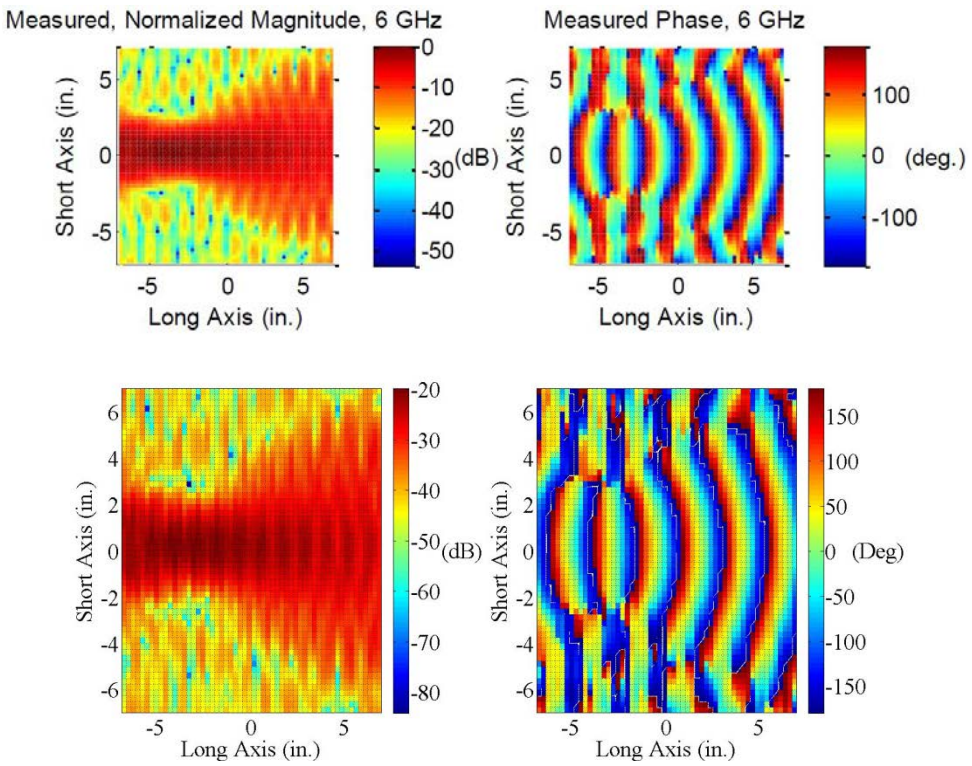

Figure 37 a) Measured (not normalized) THRU magnitude and phase for 6 GHZ with small lens b) Reported measured (normalized) magnitude and phase for 6 GHz with small lenses [8]

The D-ring measurement was performed over 2-3 GHz with a 10 MHz resolution (101 points) and both front and rear scans were performed. These near-field scans were performed over a 179 mm x 7.62 mm area with 2.54 mm spatial resolution. Figure 38 shows the D-ring measured magnitude and phase, and Figure 39 shows the previously reported data. The differences were significant in comparison to those shown by Faris. This could be due to the resolution being too great to capture the differences.

a) b)

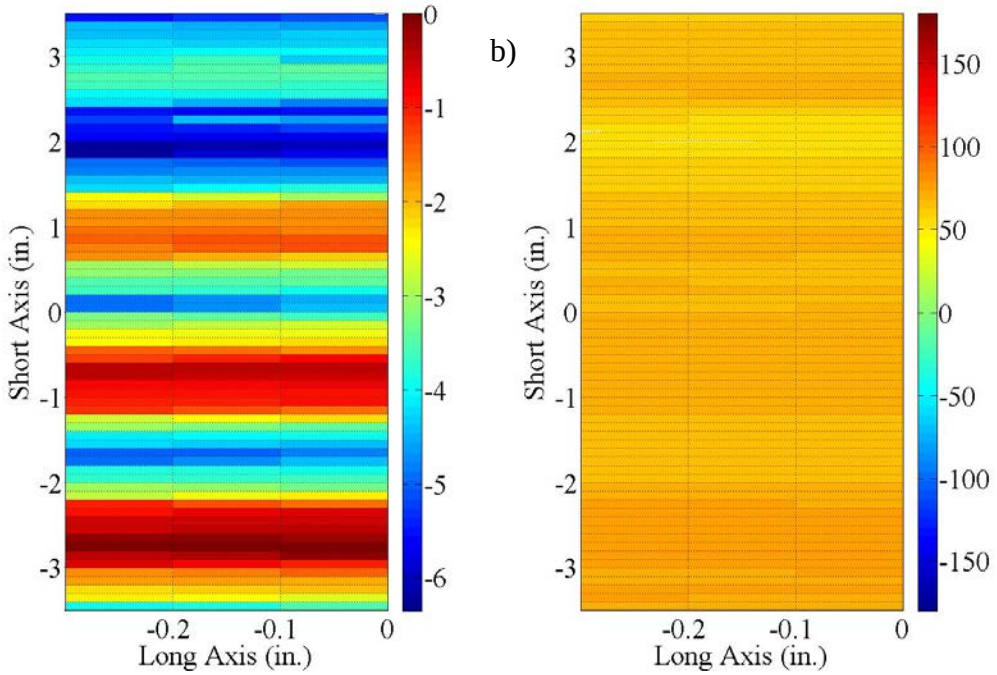

Figure 38 2 GHz frequency point from measured D-Rings centered between the small lenses a) normalized magnitude and b) phase.

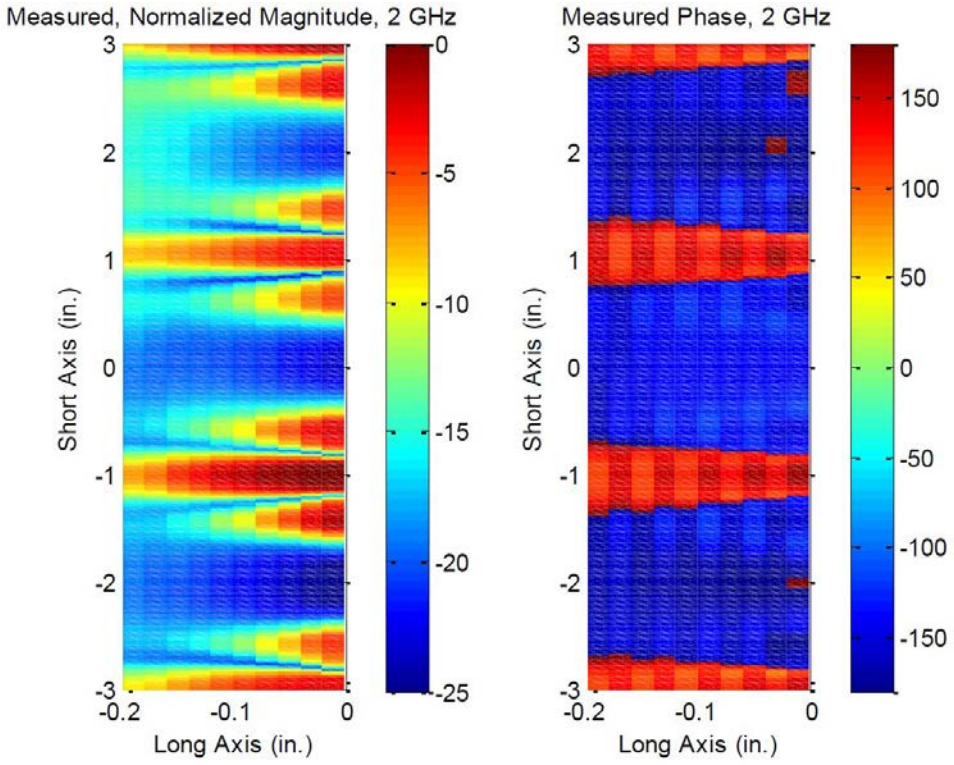

Figure 39 2 GHz frequency point from measured D-Rings centered between the small lenses reported by Faris [8].

Scattering Parameter Measurements

These measurements used both the large and small lens configurations. Each measurement was made from the left to right monopole for: the aluminum short, an acrylic sample, and the D-rings. The large lenses also included the THRU measurement since there were no near-field measurements for comparison. The frequency resolution was 10 MHz (1601 points) over the 2-18 GHz range to match the resolution used in the condensed frequency range of interest. Figure 40 through Figure 43 shows the reported measurements using the small lens configuration with the BANTAM.

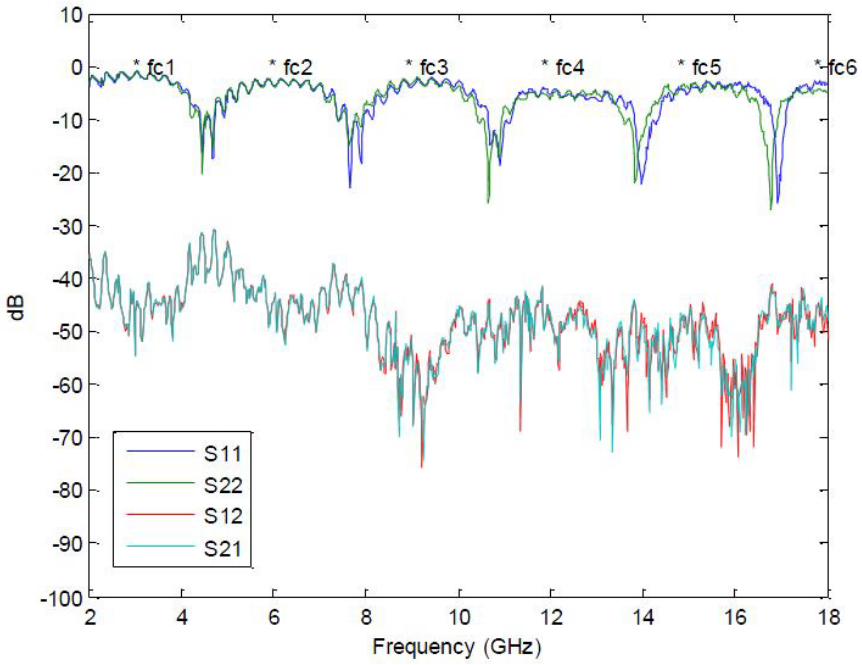

Figure 40 Measured Short s-parameters using the small lens BANTAM configuration as reported by Faris [8]

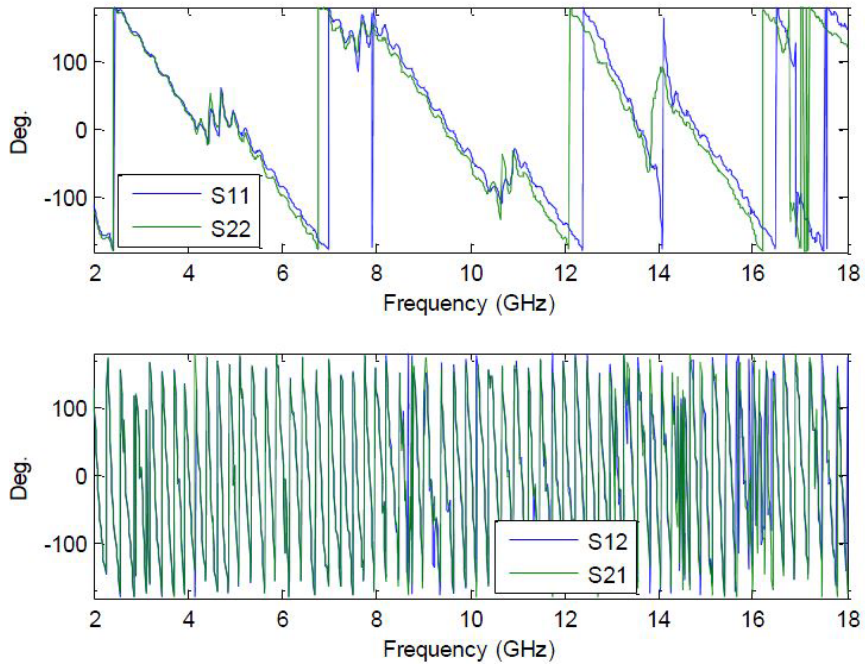

Figure 42 Phase reported for BANTAM small lens short measurement

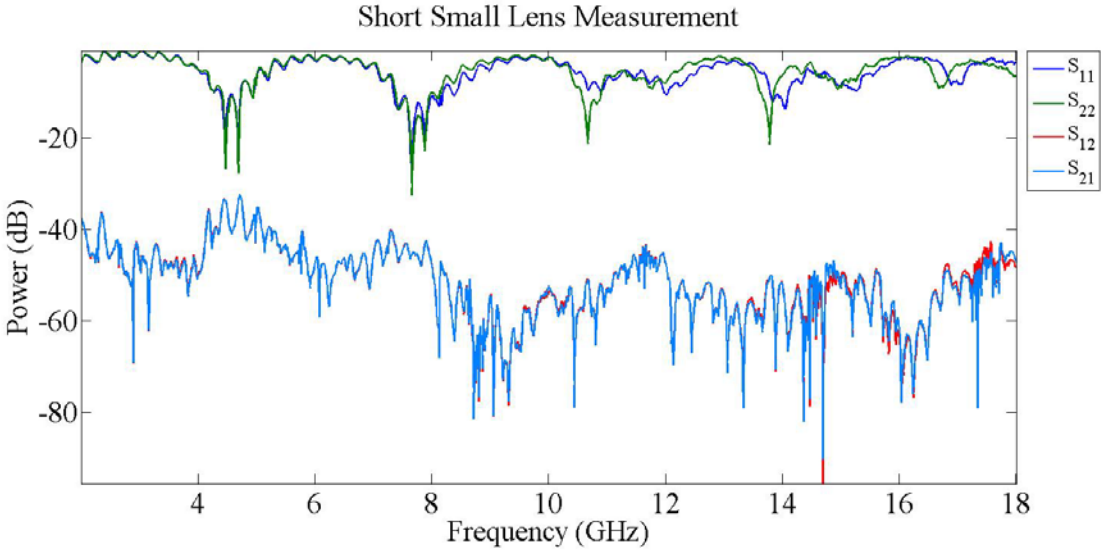

Figure 41 S-parameter measurements for the Aluminum short using the small lens configuration with BANTAM calibrated to the monopole antennas.

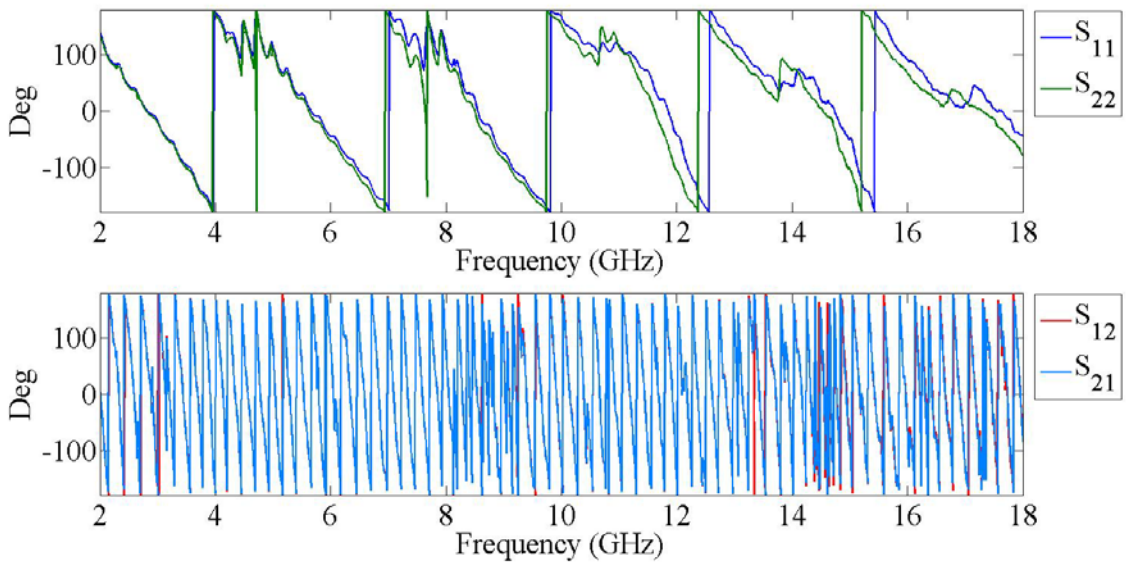

Figure 43 Phase derived from short measurement s-parameters with BANTAM small lens configuration

These measurements differ slightly in two ways. First, the last 8 GHz for the current measured short s-parameters were not as clean as those previously reported. Second, the phase we measured seemed to repeat almost twice as fast as what was previously reported. The first issue is most likely from the foam sample holders which were not part of the original measurement scheme. The phase most likely looks different because of the doubled sample points with the measurement. However, even with these differences, the cutoff frequencies were aligned. The acrylic sample measurements shown in Figure 44 through Figure 46 display even more of these differences with the small lenses.

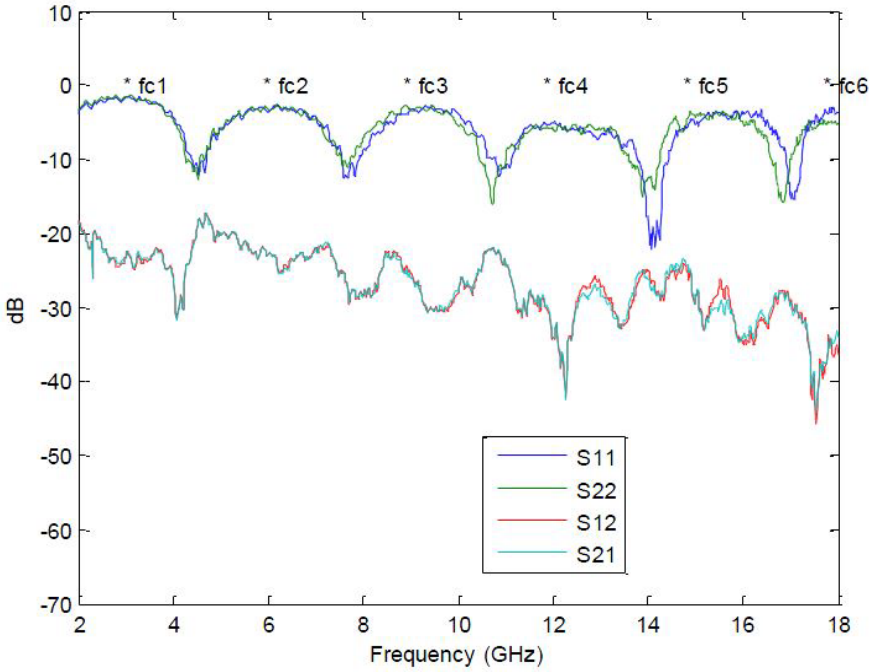

Figure 44 Reported s-parameters for acrylic sample measured with the small lens BANTAM configuration.

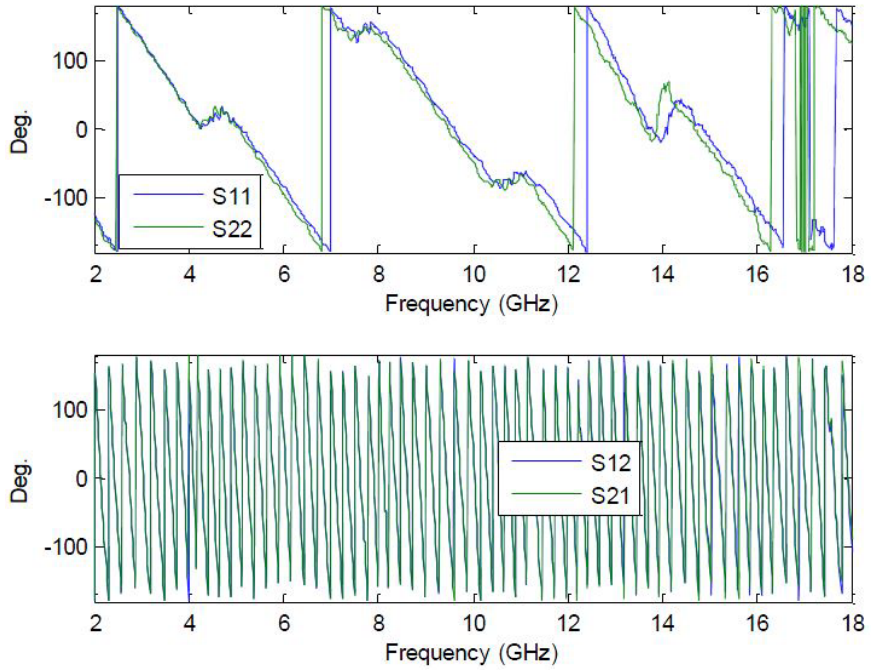

Figure 45 Reported phase from acrylic s-parameter measurements with the small lens BANTAM configuration

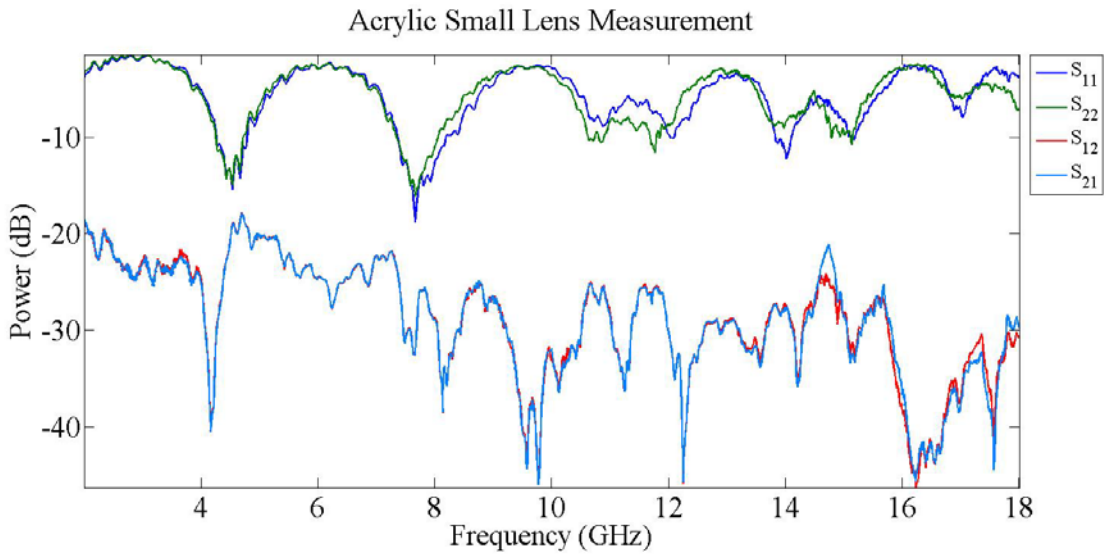

Figure 47 S-parameter measurements for acrylic sample with small lens BANTAM configuration

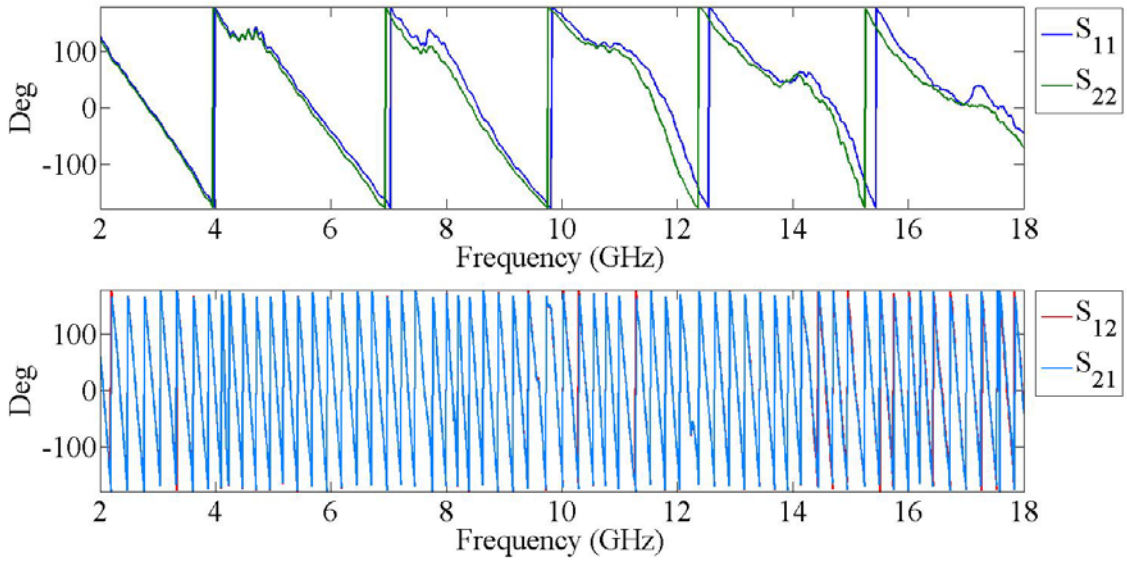

Figure 46 Phase from acrylic measurements with the small lens BANTAM configuration.

Just like the short measurements, the first 8 GHz were well aligned in magnitude and the reflection phase changes consistently one and a half times more. Then, it appears that the magnitude has two extra cut-offs at ~11.5 GHz and 14.5 GHz, which was

inconsistent with the measurements reported. However, this could be due to several differences. The first is that the monopole antennas were easily bent when changing configurations; the second is the addition of the foam sample holders, which could cause more of an effect at these higher frequencies. These effects are exactly echoed in the verification measurements and those reported by Faris shown in Figure 48 through Figure 50.

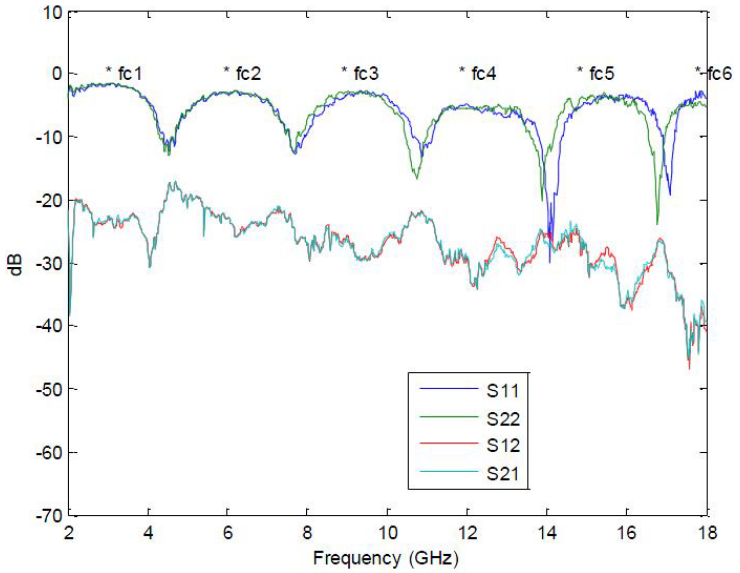

Figure 48 Reported s-parameters for D-Ring MTM measured with the small lens BANTAM configuration.

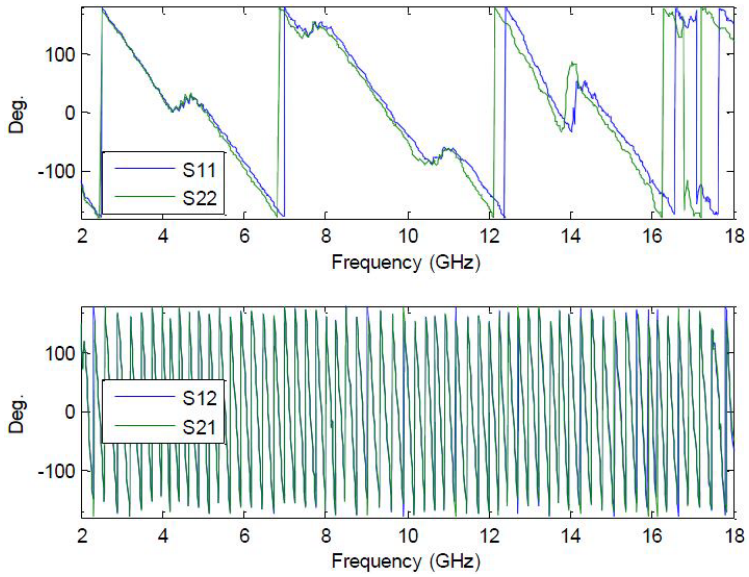

Figure 50 Reported phase from D-Ring MTM s-parameter measurements with the small lens BANTAM configuration

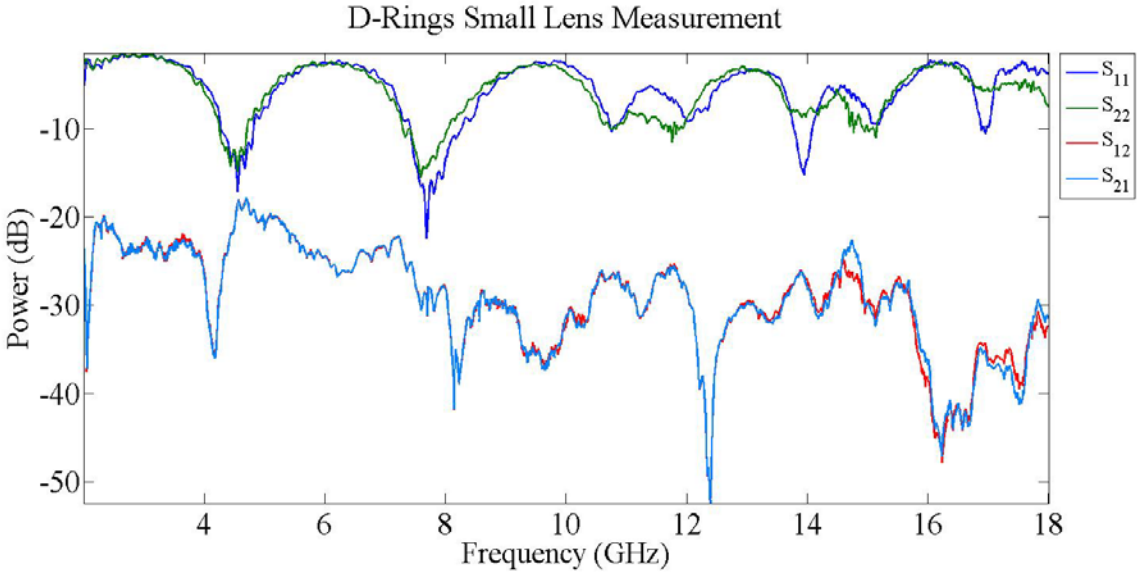

Figure 49 S-parameter measurements for D-Ring MTM with small lens BANTAM configuration

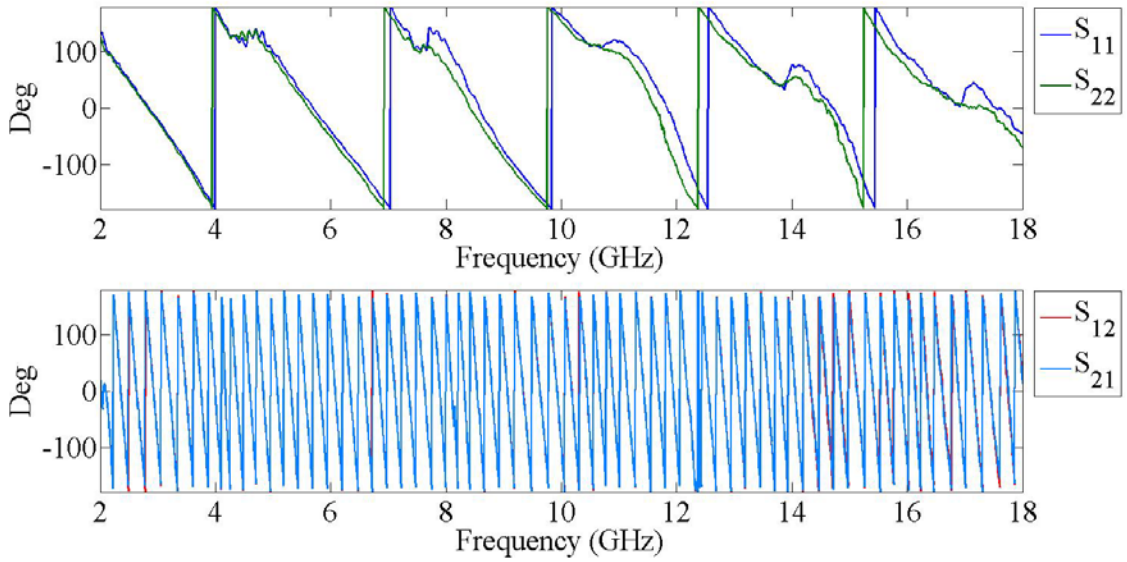

Figure 51 Phase from D-Ring MTM measurements with the small lens BANTAM configuration.

In the D-Ring MTM measurements, the 2.1 GHz resonant null is apparent in the transmission coefficients. However, just like the acrylic samples, the extra cut-offs just before 12 GHz and just after 14 GHz are visible. This reaction only seems to appear with the small lens measurements. The large lens measurements shown in Figure 52 through Figure 56 are much closer to those reported by Faris.

Large Lens Measurements (Test Points 6-9)

Only s-parameter measurements were performed with the large lenses because the antennas would be left outside of the parallel plates for top plate movements over 102 mm from center on the long axis. These measurements were from the left to right monopole, and calibrated to the cable ends with the SOLT calibration. Each of the samples discussed previously were measured, including the THRU measurement also discussed by Faris. Similar to the small lens s-parameter measurements, there is qualitatively no difference within the frequencies utilized for this research. All cut-off

frequencies measured with the large lenses appear to be comparable. The only easily distinguishable difference is the disparity between the reflection coefficients for all of the measurements that were accomplished for this research as opposed to those shown by Faris.

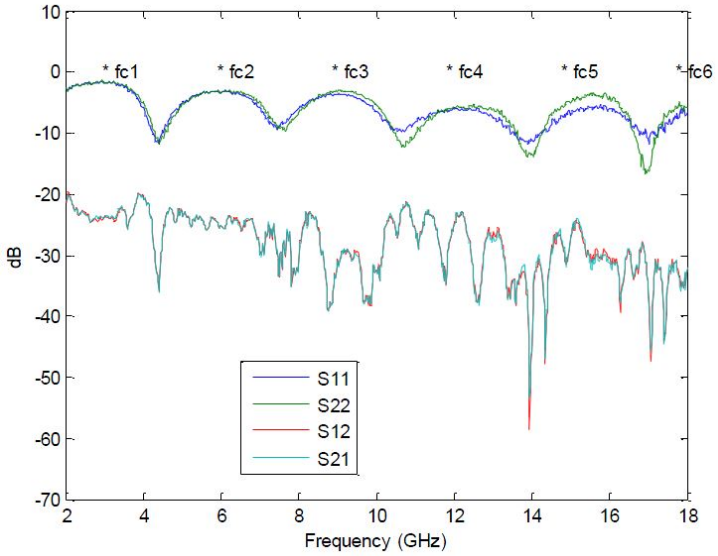

Figure 52 Reported s-parameters for THRU measurement with the large lens BANTAM configuration.

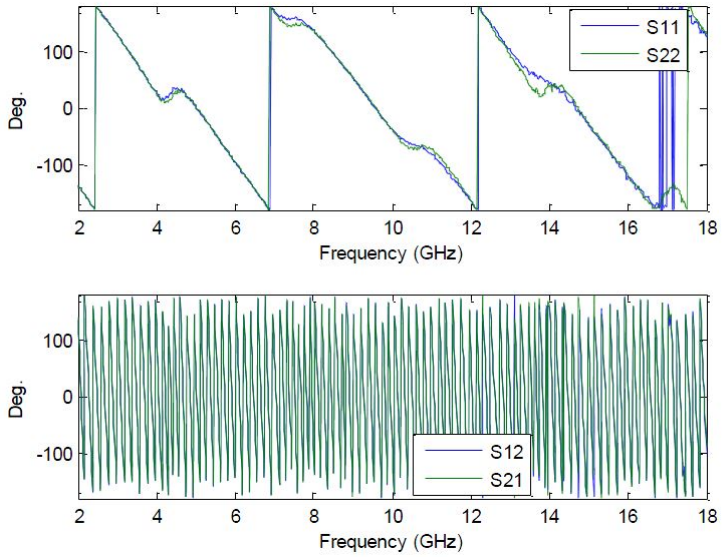

Figure 53 Reported phase from THRU s-parameter measurements with the large lens BANTAM configuration

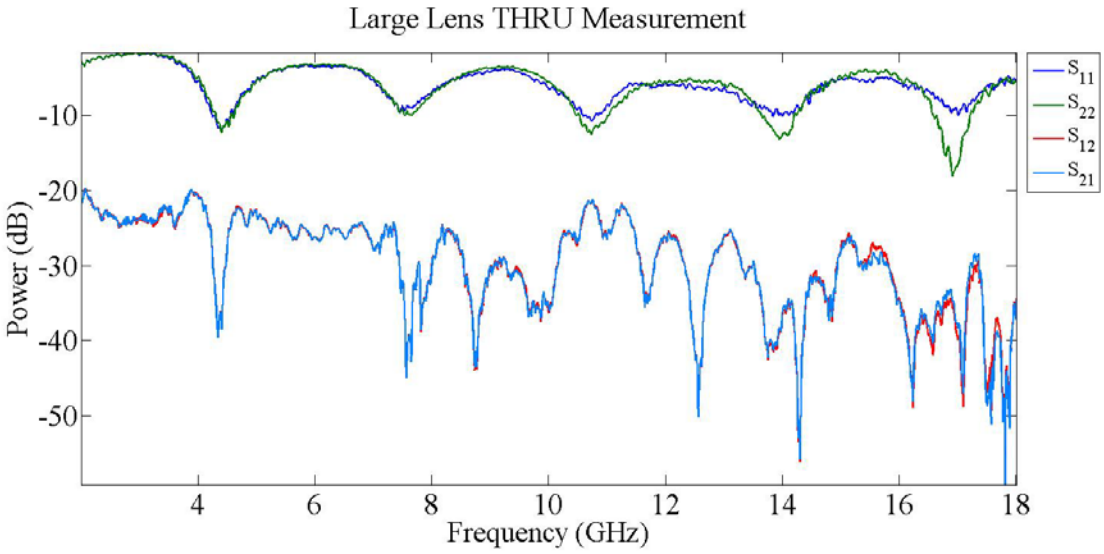

Figure 54 S-parameter THRU measurements with large lens BANTAM configuration

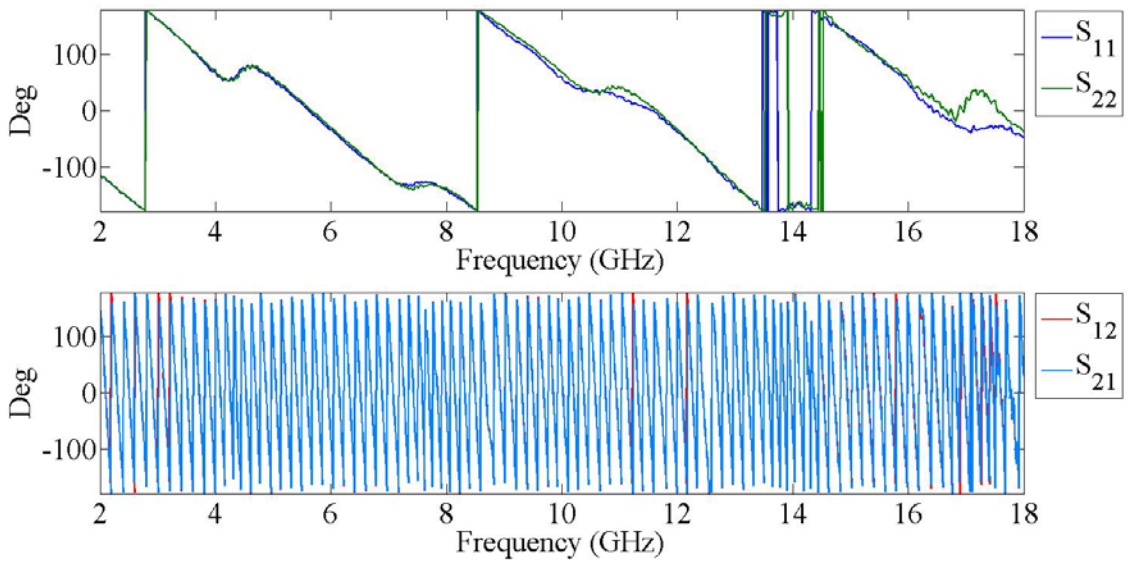

Figure 55 Phase from THRU measurements with the large lens BANTAM configuration.

Unlike many of the small lens measurements, the measured THRU magnitude in the large lens measurements matches those reported THRU magnitude. The difference is in the phase, where reflected phase frequency changes more slowly than what was reported. This effect is mimicked in test points 6-8 (short, acrylic, and d-ring MTM) as well.

The verification measurements proved that the BANTAM 2-D FBS was working as designed, at least in the frequency range of interest when the calibration and setup was accomplished as suggested. These measurements also provided an insight into the difficulties presented when accomplishing measurements with the BANTAM, as well as the possible effect of the sample holder upon measurements. Some of the issues encountered were lens drifting, cable ends breaking, and uneven lifting from the scissor lift. These issues were each fixed before moving onto MTM measurements, and provided insight into the best practices for using the BANTAM.

Appendix B

Large Lens Scattering Parameter Measurements

Large lens measurements were designed to gather s-parameter data. This measurement configuration was not recommended for using the moving top plate measurement. Therefore, this configuration was utilized to repeat the measurements Faris described [8], and to perform initial s-parameter measurements for the 2-D MTM samples. The issue with using this method for our design is twofold. The first problem is that the samples must be perpendicular to the wave front. This means that the samples point lengthwise as seen in Figure 56.

Figure 56 Large lens measurement set-up. The left monopole is connected to port 1 of the PNA and the right monopole is connected to port 2 of the PNA.

This configuration takes a large amount of space in order to achieve desired spacing of meta-atom arrays between the lenses. To take proper measurements the amount of meta-atoms for the metamaterial were reduced from eight to four which is depicted in Figure 56. The second problem comes from the beamwaist which, at the

frequencies of interest, can be up to 279 mm. This size is a problem because the meta-atom arrays were spaced ~10mm apart from each other. Therefore, to fill just the beamwaist 28 arrays would be required. To cross the entire PPWG 82 meta-atom arrays would be required (approximately 32" across or 812mm), and that amount of meta-atoms is prohibitively time consuming and costly to produce for one material, let alone three. These limitations are unfortunate because the benefit derived from using the large lenses is a larger measurement space which allows the freedom to have a longer sample than the small lenses allow.

After the verification measurements were made, the metamaterial measurements were performed in several configurations as laid out in Table 8. These tests started with previously reported materials for material property extraction purposes. The verifications-parameter measurements were followed with the s-parameter measurements for the three MTM frequencies designed.

Table 8 Metamaterial and material property extraction measurement test points

Test Point	Configuration	Description
1	Large Lens	Left-right (Post Cal THRU)
2	Large Lens	Left-right (Acrylic)
3	Large Lens	Left-right (D-Rings)
4	Large Lens	Left-right (Cu on FR4 MTM Line)
5	Large Lens	Left-right (Cu on FR4 MTM Box)

The purpose of the large lens measurements was to prove the viability of the BANTAM for use in material property extraction for larger material samples. The measurements in Table 8 were each performed within the 2-3 GHz range. This range was chosen in order to stay within the fundamental mode to utilize the NRW material

property extraction. Frequency resolution was set to 1 MHz, and the three-short calibration was first utilized for these measurements.

Initially four main measurements were to be performed to compare the relative EM properties: 1) empty (THRU), 2) 2 GHz SRR MTM, 3) D-Ring MTM, and 4) Acrylic. Ideally, the THRU measurement validates the calibration method as seen in Figure 54. Then the s-parameters from the two different MTM designs could be compared to each other and relative to a simple dielectric material (the acrylic sample shown in Figure 60compared to the MTM samples in Figure 59 and Figure 58).

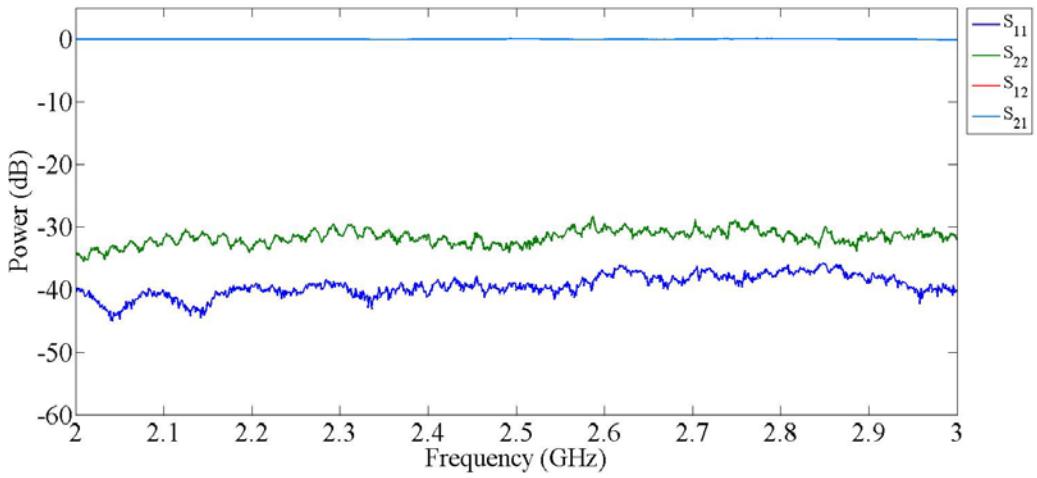

Figure 57 THRU measurement with large lens BANTAM configuration

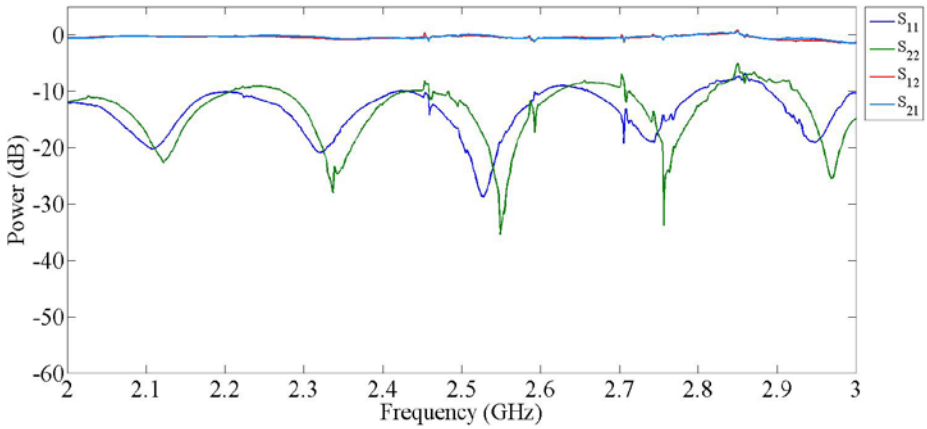

Figure 60 Acrylic measurement with large lens BANTAM configuration

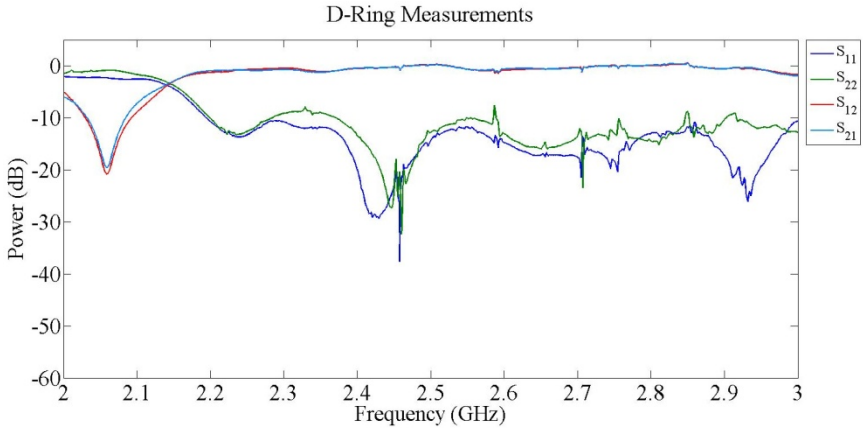

Figure 59 D-Ring MTM measurement with large lens BANTAM configuration

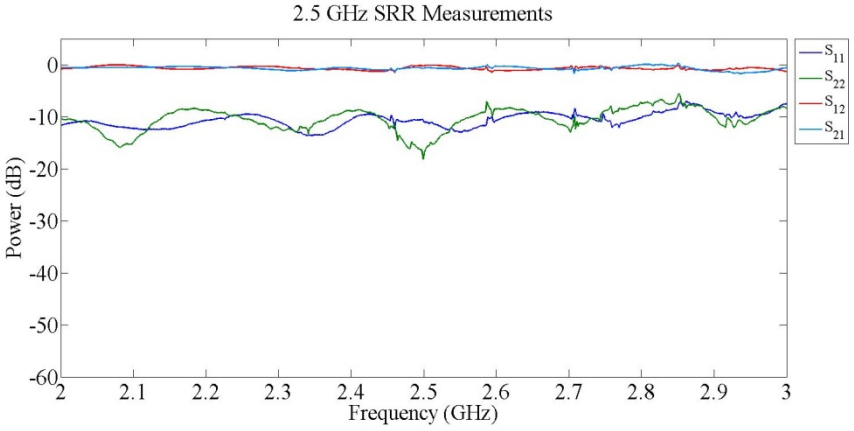

Figure 58 2.5 GHz MTM design measurement aligned in a line like D-Ring measurement with large lens BANTAM configuration

The first issue was that the SRR design chosen has a very directional response. This meant that the MTM sample could not be placed in the same configuration. Moreover, the amount of material needed for this configuration was prohibitive, so to show the directivity of the SRR design, a "box" sample was tested for comparison. Figure 61 shows the resulting measurement. Due to the lack of response, and the highly anisotropic reflection response, the null is outlined.

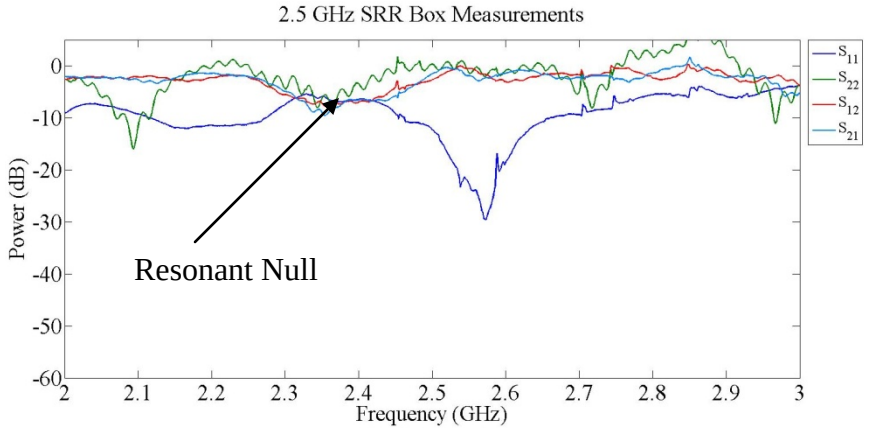

Figure 61 Large lens s-parameter measurements for 2.5 GHz MTM design formed into a box aligned to the center between the large lenses

The d-ring metamaterial measurement shows its suitability for this measurement configuration with -21 dB null and associated reflection at ~0 dB. This is drastically opposite to the initial design measurement, which appears to be exactly the same as the acrylic sample. However, even with the box change the resonance is barely -10 dB for the null and the reverse reflection is completely incoherent.

One other issue that is apparent throughout all of the s-parameters shown in Figure 54 through Figure 61 is the noise along the measurement. This is due to the lack of gating from the PNA. The solution comes in the form of post process gating. To verify the length of time gating needed, three short measurements were employed to see

where the sample was in time and where the other parts of the measurement device were interfering. Figure 62shows the short measurements in the time domain and illustrate the movement of the short through the BANTAM.

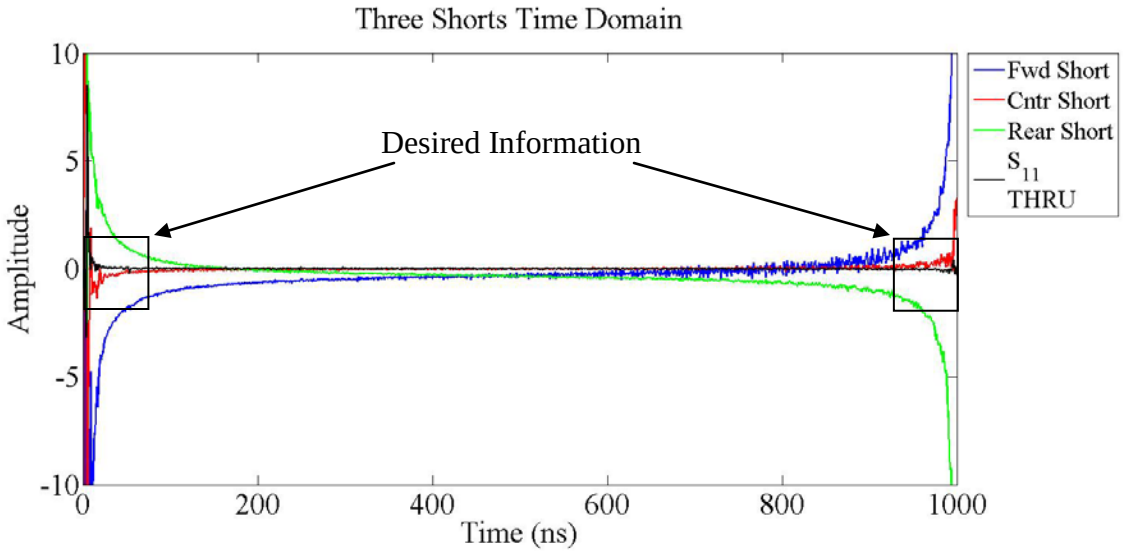

Figure 62 Inverse Fast Fourier transformed s-parameters showing time domain response for the three short measurements measured with forward reflection

Using the time location of the short at the center, which is at the calibration plane, at time zero we can see that the forward time gating can be the first 55 ns and the last 44 ns. This was optimized to be 15 ns front and 5 ns rear time gating. This gating was employed with the MTM boxes, D-rings and acrylic for comparison; Figure 63, Figure 64, and Figure 65 show the results.

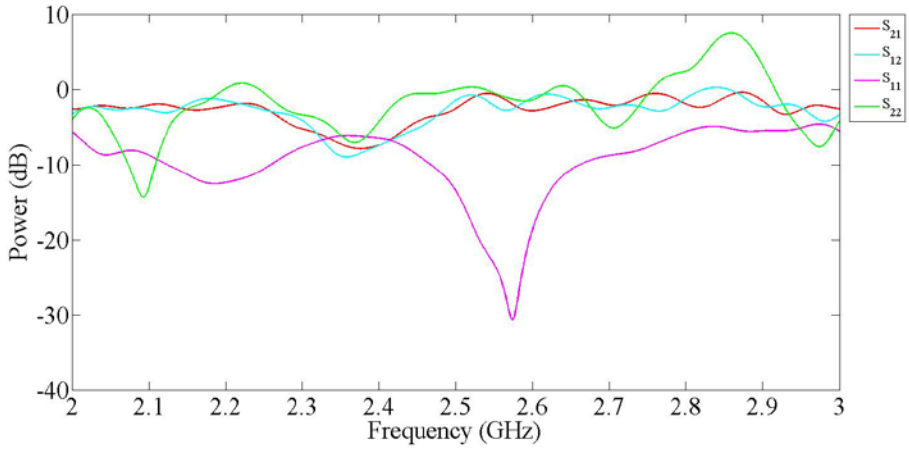

Figure 63 2.5 GHz MTM Box measurement post gating for gating at 14 ns in front and 5 ns at the rear

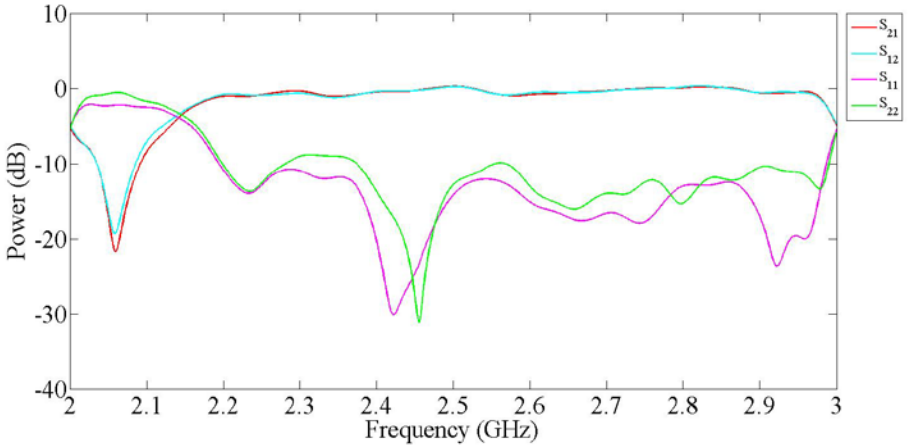

Figure 64 D-Ring MTM measurement post gating for gating at 14 ns in front and 5 ns at the rear

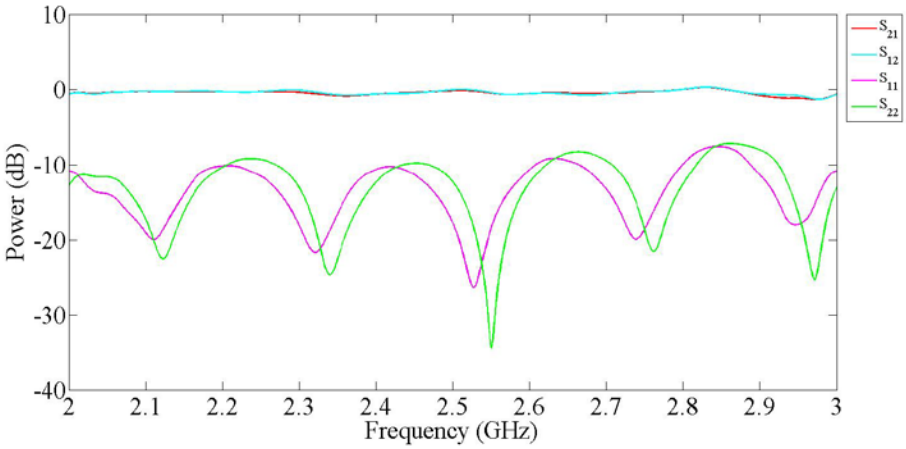

Figure 65 Acrylic measurement post gating for gating at 14 ns in front and 5 ns at the rear

These samples highlight the benefit of time domain gating to help achieve optimal measurements. The resonant null becomes more obvious in both the MTM and the d-rings, and the acrylic sample shows less noise across all of the s-parameters. This effect however, is not as apparent in the material property extraction, which still demonstrates the problems with utilizing this measurement method.

References

[1] T. Itoh and C. Caloz, Electromagnetic Metamaterials: Transmission Line Theory and Microwave Applications, London: Wiley-Interscience, 2006.

[2] E. Solymar and L. Shamonina, "Metamaterials: How the subject started," *Metamaterials,* vol. 1, no. 1, pp. 12-18, 2007.

[3] D. R. Smith and R. Liu, Metamaterials: Theory, Design, and Applications, Springer Science+Business Media, 2010.

[4] V. G. Veselago, "The Electrodynamics of Substances with Simultaneously Negative Values of ε and μ," *Soviet Phys. Usp.,* vol. 10, no. 4, pp. 509-514, 1968.

[5] J. B. Pendry, A. J. Holden, W. J. Stewart and I. Young, "Extremely Low Frequency Plasmons in Metallic Mesostructures," *Physics Review Letters,* vol. 76, no. 25, pp. 4773-4776, 1996.

[6] J. B. Pendry, A. J. Holden, D. J. Robbins and W. J. Stewart, "Magnetism from Conductors and Enhanced Nonlinear Phenomena," *IEEE Trans. Microw. Theory Tech.,* vol. 47, no. 11, pp. 2075-2084, 1999.

[7] D. R. Smith, W. J. Padilla, D. C. Vier, S. C. Nemat-Nasser and S. Schultz, "Composite Medium with Simultaneous Negative Permeability and Permitivity," *Physical Review Letters,* vol. 84, no. 11, pp. 4184-4187, 2000.

[8] S. I. Faris, "Development of a Radar-Frequency Metamaterial Measurement and Characterization Apparaus," *M.S. thesis,* 2012.

[9] X. Chen, T. M. Grzegorczyk, B. Wu, J. Pacheco and J. A. Kong, "Robust Method to Retrieve the Constitutive Effective Parameters of Metamaterials," *Physical Review Letters,* vol. 70, no. 016608, pp. 1-7, 2004.

[10] D. Langley, "Design, Fabrication, and Testing of Tunable RF Meta-Atoms," *Ph.D. dissertation,* 2012.

[11] T. Le, Z. Lin, R. Vas, L. Vasileios, L. Yang, A. Traille, M. M. Tentzeris and C.-p. Wong, "Inkjet Printing of Radio Frequency Electronics: Design Methodologies

and Application of Novel Nanotechnologies," *Journal of Electronic Packaging,* vol. 135, no. 011007, pp. 1-14, 2013.

[12] W. E. Gunn Jr., "Application of the Three Short Calibration Technique in a Low Frequency Focus Beam System," *M.S. thesis,* 2010.

[13] L. Rederus, "A MEMS Multi-Cantilever Variable Capacitor on Metamaterial," *M.S. thesis,* 2009.

[14] F. Bilotto, M. Barbuto, L. Di Palma, D. Ramaccia, A. Toscano and L. Vegni, "Linear and Circular Polarized Electrically Small Antennas Based on the Employment of Metamaterial-Inspired Sub-Wavelength Resonators," in *7th European Conference on Antennas and Propogation,* Gothenburg, 2013.

[15] M. Yoo and L. Sungjoon, "Wideband Metamaterial Absorber using an RC Layer," in *2013 Asia-Pacific Microwave Conference,* Seoul, 2013.

[16] J. R. A. Coutu, P. J. Collins, E. A. Moore, D. Langley, M. E. Jussaume and L. A. Starman, "Electrostatically Tunable Meta-Atoms Integrated With In-Situ Fabricated MEMS Cantilever Beam Arrays," *JMEMS,* pp. 1-6, 2011.

[17] J. B. Pendry, "Negative Refraction Makes a Perfect Lens," *Physical Review Letters,* vol. 85, no. 18, pp. 3966-3969, 2000.

[18] D. Schurig, J. J. Mock, B. J. Justice, S. A. Cummer, J. B. Pendry, A. F. Starr and D. R. Smith, "Metamaterial Electromagnetic Cloak at Microwave Frequencies," *Science,* vol. 314, no. 5801, pp. 977-980, 2006.

[19] C. M. Watts, X. Liu and W. J. Padilla, "Metamaterial Electromagnetic Wave Absorbers," *Advanced Optical Metamaterials,* vol. 24, pp. 98-120, 2012.

[20] M. E. Jussaume, "Electromagnetic Modeling and Measurement of Adaptive Metamaterial Structural Elements," *M.S. thesis,* 2011.

[21] D. R. Smith, S. Schultz, P. Markos and C. M. Soukoulis, "Determination of Effective Permittivity and Permeability of Metamaterials from Reflection and Transmission Coefficients," *Phyical Review B,* vol. 64, no. 195104, pp. 1-5, 2002.

[22] G. W. Hanson, J. M. Grimm and D. P. Nyquist, "An Improved De-Embedding Technique for the Measurement of the Complex Constitutive Parameters of Materials Using a Stripline Field Applicator," *IEEE Tran. on Inst. and Meas.,* vol. 42, no. 3, 1993.

[23] S. He and T. Chen, "Broadband THz Absorbers with Graphene-Based Anisotropic Metamaterial Films," *IEEE Transactions on Terahertz Science and Technology,* vol. 3, no. 6, pp. 757-763, 2013.

[24] Z. N. Chen, Y. Sun, Nasimuddin, P. Y. Lau, X. Qing and Y. Zhang, "Metamaterials-based High-gain PlanarAntennas," in *2012 International Conference on Microwave and Millimeter Wave Technology (ICMMT)*, Shenzhen, 2012.

[25] S.-T. Ko, B.-C. Park and J.-H. Lee, "Dual-band Circularly Polarized Hybrid Metamaterial Patch Antenna," in *2013 Asia-Pacific Microwave Conference*, Seoul, 2013.

[26] B. D. Bala, M. K. A. Rahim, N. A. Murad, M. F. Ismail and H. A. Majid, "Design and Analysis of Metamaterial Antenna Using Trinagular Resonator," in *2012 Asia-Pacific Microwave Conference*, Kaohsiung, 2012.

[27] S. Kim, Y. Kawahara, A. Georgiadis, A. Collado and M. M. Tentzeris, "Low-cost inkjet-printed fully passive RFID tags using metamaterial-inspired antennas for capacitive sensing applications," in *2013 IEEE MTT-S International Microwave Symposium Digest*, Seattle, 2013.

[28] J.-H. Lee, S.-T. Ko and B.-C. Park, "Hybrid Metamaterial Antennas," in *43rd European Microwave Conference*, Nuremberg, 2013.

[29] T. Kokkinos and A. P. Feresidis, "Electrically Small Superdirective Endfire Arrays of Metamaterial-Inspired Low-Profile Monopoles," *IEEE Antennas and Wireless Propogation Letters,* vol. 11, pp. 568-571, 2012.

[30] Y. Dong and T. Itoh, "Metamaterial-Based Antennas," *Proceedings of the IEEE,* vol. 100, no. 7, pp. 2271-2285, 2012.

[31] C. Caloz, T. Itoh and A. Rennings, "CRLH Metamaterial Leaky-Wave and Resonant Antennas," *Antennas and Propogation Magazine*, vol. 50, no. 5, pp. 25-39, 2008.

[32] A. M. H. Wong and G. V. Eleftheriades, "Advances in Imaging Beyond the Diffraction Limit," *IEEE Photonics Journal,* vol. 4, no. 2, pp. 586-589, 2012.

[33] T. N. Duong, J. Venkararaman and Z. Lu, "Enhancement of Ambient Energy Harvesting Using a Metamaterial Lens," in *2013 IEEE Antennas and Propagation Society International Symposium*, Orlando, 2013.

[34] J. P. Turpin, Q. Wu, D. H. Werner, B. Martin, M. Bray and E. Lier, "Low Cost and Broadband Dual-Polarization Metamaterial Lens for Directivity Enhancement," *IEEE Transactions on Antennas and Propagation,* vol. 60, no. 12, pp. 5717-5726, 2012.

[35] C. Mutzel, S. MacNaughton and S. Sonkusale, "Paint-On Metamaterial: Low Cost Fabrication of Absorbers at X Band Frequencies," in *2012 IEEE MTT-S International Microwave Symposium Digest*, Montreal, 2012.

[36] B. S. Cook and A. Shamim, "Utilizing Wideband AMC Structures for High-Gain Inkjet-Printed Antennas on Lossy Paper Substrate," *IEEE Antennas and Wireless Propagation Letters,* vol. 12, pp. 76-79, 2013.

[37] N. Engheta and R. Ziolkowski, Metamaterials: Physics and Engineering Explorations, London: Wiley-Interscience, 2006.

[38] E. A. Ruehli, "Inductance Calculations in a Complex Integrated Circuit Environment," *IBM Journal of Research and Development,* vol. 16, no. 5, pp. 470-481, 1972.

REPORT DOCUMENTATION PAGE

Form Approved
OMB No. 074-0188

1. REPORT DATE *(DD-MM-YYYY)*	2. REPORT TYPE	3. DATES COVERED *(From – To)*
03-03-2014	Master's Thesis	August 2012 – March 2014

TITLE AND SUBTITLE

DESIGN, FABRICATION AND TESTING OF TWO DIMENSIONAL RADIO-FREQUENCY METAMATERIALS

5a. CONTRACT NUMBER

5b. GRANT NUMBER

5c. PROGRAM ELEMENT NUMBER

6. AUTHOR(S)

Krones, Russell P., Captain, USAF

5d. PROJECT NUMBER

5e. TASK NUMBER

5f. WORK UNIT NUMBER

7. PERFORMING ORGANIZATION NAMES(S) AND ADDRESS(S)
Air Force Institute of Technology
Graduate School of Engineering and Management (AFIT/ENY)
2950 Hobson Way, Building 640
WPAFB OH 45433-8865

8. PERFORMING ORGANIZATION REPORT NUMBER

AFIT-ENG-14-M-45

9. SPONSORING/MONITORING AGENCY NAME(S) AND ADDRESS(ES)
Intentionally left blank

10. SPONSOR/MONITOR'S ACRONYM(S)

11. SPONSOR/MONITOR'S REPORT NUMBER(S)

12. DISTRIBUTION/AVAILABILITY STATEMENT
DISTRUBTION STATEMENT A. APPROVED FOR PUBLIC RELEASE; DISTRIBUTION UNLIMITED.

13. SUPPLEMENTARY NOTES
This material is declared a work of the U.S. Government and is not subject to copyright protection in the United States.

14. ABSTRACT
This project focused on radio frequency (RF) metamaterials (MTM) structures using two different methods: wet etching copper (Cu) on insulating glass reinforced epoxy resin (FR4) and silver nano-particle ink printed SRR meta-atoms on photo paper (Ag on paper). Once the MTMs were fabricated, RF properties were measured using a 0-4 GHz stripline and the 2-18 GHz broad antenna near-field test and measurement range two dimensional focus beam system. Through electromagnetic (EM) material property extraction of these RF measurements, the EM properties of the MTM were also shown. Three tests were employed: scattering parameter measurements, near-field testing, and empty PPWG application testing. Results from the RF testing showed that the highest performing MTM was the Ag on paper with FR4 backing. These devices performed closest to analytic modeling and showing resonance within .4% of simulations (2.56 GHz to 2.57 GHz). This sample also displayed the best null at -21 dB, which was 3 dB lower than the Cu on FR4. These results could be used in a number of applications, including RF absorbers or RF cloaking devices. We have successfully shown a fully capable metamaterial testing system including material property extraction.

15. SUBJECT TERMS
Meta-atom, metamaterial, radio frequency, RF, RF testing, RF measurement

16. SECURITY CLASSIFICATION OF:			17. LIMITATION OF ABSTRACT	18. NUMBER OF PAGES	19a. NAME OF RESPONSIBLE PERSON
a. REPORT	b. ABSTRACT	c. THIS PAGE			Derrick Langley, CAPT, USAF, AFIT/ENG
U	U	U	UU	114	19b. TELEPHONE NUMBER *(Include area code)* (937) 785-3636, ext 6165 (NOT DSN) (derrick.langley@us.af.mil)

Standard Form 298 (Rev. 8-98)
Prescribed by ANSI Std. Z39-18